RSC Advances

PAPER

View Article Online
View Journal | View Issue

Cite this: *RSC Adv.*, 2024, **14**, 26674

Design, synthesis, anticancer and *in silico* assessment of 8-caffeinyl chalcone hybrid conjugates†

Mohammad Navid Soltani Rad, *[ab] Somayeh Behrouz, *[ab] Maedeh Charbaghi,[a] Marzieh Behrouz,[a] Elham Zarenezhad[c] and Ali Ghanbariasad[d]

In this paper, we report the design, synthesis, and characterization of novel 8-caffeinyl chalcone hybrid conjugates, which were studied for their anticancer properties, toxicity, and *in silico* behavior. The synthesized compounds consist of 8-caffeinyl and chalcone structures with diverse substituents. The synthesis involved three main stages: bromination of caffeine to produce 8-BC, synthesis of chalcones, and subsequent coupling of these chalcones with 8-BC. The anticancer activity of the resulting compounds was evaluated *in vitro* against breast cancer MCF-7 and melanoma A-375 cell lines, revealing certain compounds to have significant efficacy compared to the reference drug methotrexate. Toxicity assessments using a healthy cell line indicated that most compounds displayed some level of toxicity, with only a few exceptions. Molecular docking studies indicated robust binding affinities of selected compounds to B-RAF kinase and hDHFR enzymes. *In silico* analyses of pharmacokinetic and physicochemical properties demonstrated that the majority of the compounds adhered to Lipinski's rule of five. Furthermore, density functional theory (DFT) studies were performed to gain deeper insights into the properties of the intermediates used throughout the research.

Received 2nd July 2024
Accepted 16th August 2024

DOI: 10.1039/d4ra04787g

rsc.li/rsc-advances

1. Introduction

Cancer, the second leading cause of death globally following cardiovascular disease, is a complex condition characterized by the uncontrolled proliferation of abnormal cells in the body.[1] In 2017 alone, it resulted in over 9.6 million deaths worldwide, with projections indicating that global cancer-related mortality could reach 22 million by 2030.[2] Despite significant advancements in understanding cancer development and treatment in recent years, the disease remains challenging to manage due to factors such as tumor heterogeneity, genetic mutations, and its ability to affect various cells and organs.[3] Cancer is a dynamic ailment that evolves over time, accumulating new mutations, making clinical management a persistent challenge in the 21st century. Treatment options include radiation therapy, surgery, chemotherapy, and proton therapy, with the choice of therapy tailored to the cancer type and stage.[4] While surgery is typically the primary treatment, advanced stages often require a combination of radiotherapy and chemotherapy. However, these treatments can cause significant damage to surrounding healthy tissues, leading to long-term complications such as neurotoxicity, cardiotoxicity, and infertility. Furthermore, chemotherapeutic agents have been associated with various drawbacks such as lack of selectivity, low efficacy, high prices, inconsistency, and other issues. Hence, efforts are ongoing to develop more effective and less toxic drugs to address the limitations associated with current cancer treatments.[5]

Chalcones, specifically 1,3-diphenylprop-2-en-1-one, are a type of open-chain flavonoid featuring an α,β-unsaturated carbonyl group. They serve as fundamental structures in various natural compounds and play a vital role as precursors for the biosynthesis of flavonoids and isoflavonoids from both natural and synthetic sources within the flavonoid family.[6] These compounds come in trans and cis isomeric forms, with the trans isomer being more thermodynamically stable. They are predominantly found in plant species like *Angelica*, *Glycyrrhiza*, *Humulus*, and *Scutellaria*, which have a history of use in traditional folk remedies.[7] Many derivatives of chalcones have been created and approved for medicinal use. Researchers have been intrigued by chalcones due to their simple chemistry, ease of synthesis, and the ability to produce a wide range of derivatives by replacing multiple hydrogen atoms.[8] Because of their abundance in plants and ease of production, these compounds have

[a]*Department of Chemistry, Shiraz University of Technology, Shiraz, 71555-313, Iran. E-mail: soltani@sutech.ac.ir; behrouz@sutech.ac.ir; Fax: +98-71-3735-4520; Tel: +98-71-3735-4500*

[b]*Medicinal Chemistry Research Laboratory, Novel Technology for Health Research Center, Shiraz University of Technology, Shiraz, 71555-313, Iran*

[c]*Non-communicable Diseases Research Center, Fasa University of Medical Sciences, Fasa, Iran*

[d]*Department of Medical Biotechnology, School of Medicine, Fasa University of Medical Sciences, Fasa, Iran*

† Electronic supplementary information (ESI) available. See DOI: https://doi.org/10.1039/d4ra04787g

attracted significant attention for potential therapeutic applications. Numerous chalcone derivatives have been synthesized in laboratories, showcasing diverse biological activities such as anti-diabetic, anti-neoplastic, antihypertensive, anti-retroviral, anti-inflammatory, and many others (Fig. 1).[9] In recent years, several comprehensive reviews have emphasized the biological importance of chalcone derivatives, particularly those containing N-heterocyclic compounds known for their exceptional biological properties.[10]

Xanthine alkaloids are a group of compounds with notable significance due to their wide-ranging biological activities and pharmacological effects.[11] These alkaloids, including caffeine, theophylline, paraxanthine, and theobromine (Fig. 2), are found in various plants such as coffee, tea, and cacao. They act as central nervous system stimulants, diuretics, and bronchodilators, making them commonly used in medicine and as psychoactive substances. Xanthine alkaloids also play a crucial role in plant defense mechanisms and have antioxidant properties. Their impact on human health and their diverse physiological effects makes xanthine alkaloids a subject of significant scientific interest and research.[12]

Caffeine stands out as the most well-known and widely used natural xanthine alkaloid in human society, with established biological properties.[13] Unlike other *N*-methyl xanthines, caffeine can be uniquely modified at its C8 site by a select few electrophiles or active species.[14] Notably, functionalizing the C8 position of caffeine leads to significant changes in its biological characteristics, offering a range of medicinal properties as illustrated in Fig. 3. A recent study has classified C8-modified

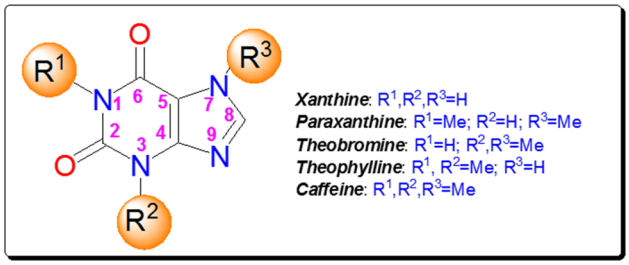

Fig. 2 The structures of xanthine and its natural methylated derivatives.

caffeine derivatives into C8–C, C8–O, C8–S, and C8–N based on the type of atom linked to C8.[15] Among these derivatives, C8–O analogues exhibit remarkable biological activities, including anticancer, antimicrobial, analgesic, MAO and adenosine inhibitors.[16–18] Contrary to C8–C, C8–S, and C8–N modified derivatives, the synthesis of C8–O analogues has been rare. Fig. 4 showcases the structures and biological activities of some C8–O derivatives **1–3**.

A hybrid conjugate compound is an artificial combination of two or more pharmacophores that fall into a known category of compounds for producing the desired effect. Hybrid conjugates play a crucial role in various fields, including chemistry, biology, and medicine.[19] These molecules combine different properties and functionalities, resulting in enhanced performance and versatility. These synthetic structures have the potential to generate novel chemotherapeutic agents that

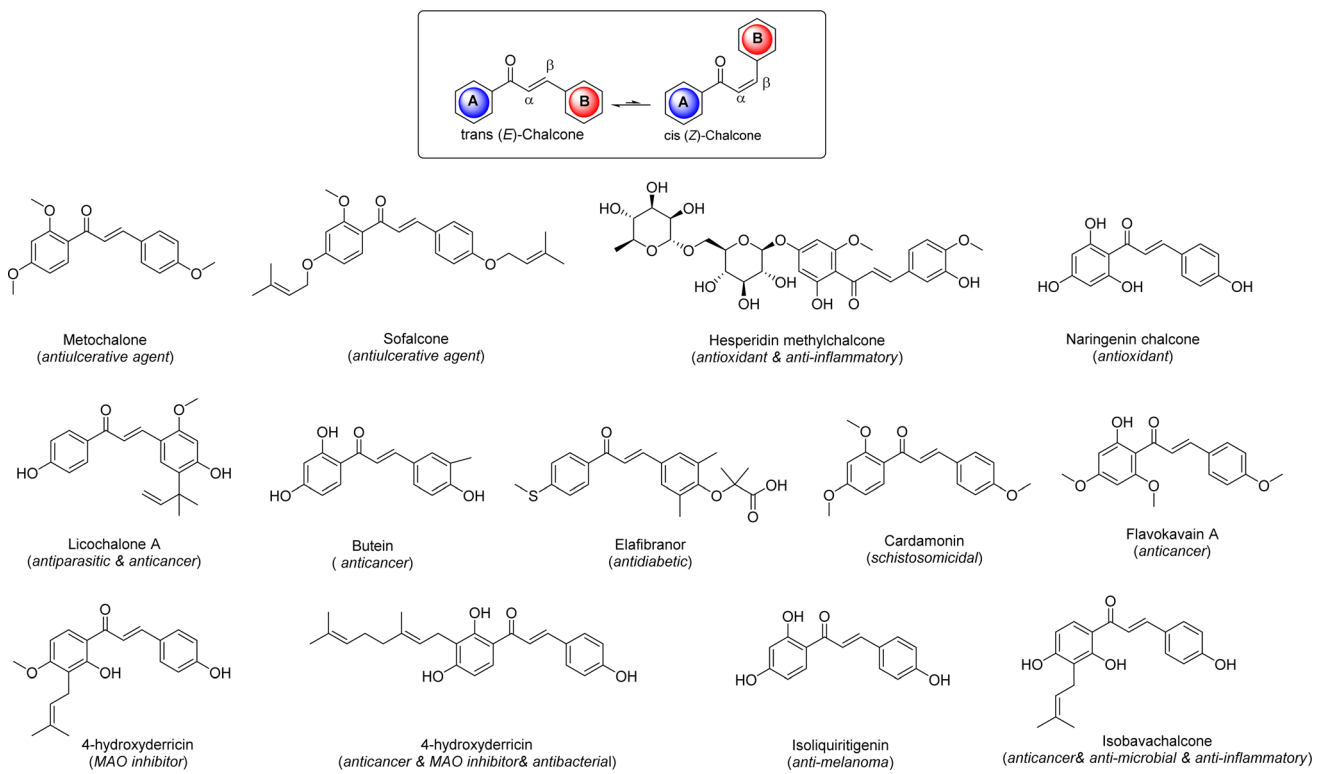

Fig. 1 The structures of chalcone and chalcone scaffold-based drugs.

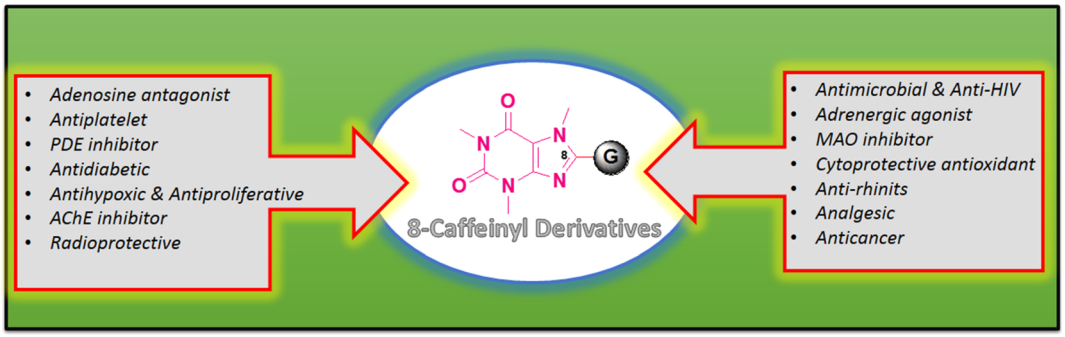

Fig. 3 The biological profiles obtained by the C8 modification of caffeine.

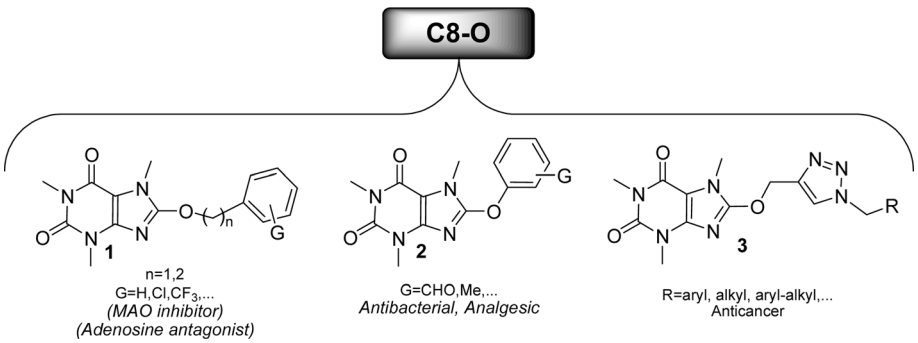

Fig. 4 The structure of some C8–O caffeine derivatives and their corresponding biological activity.

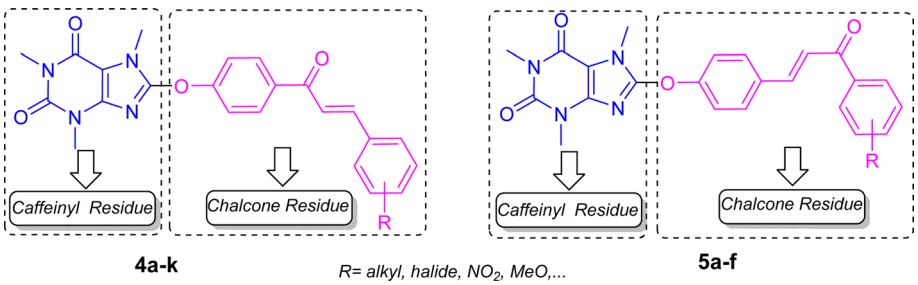

Fig. 5 General structure of novel 8-caffeinyl chalcone hybrid conjugates.

enhance efficacy and activity, improve binding affinity, extensively improve drug delivery, and reduce side effects.[20] Through scientific innovation, molecular hybrids have been developed by linking different biologically active agents together with the goal of preserving the pharmacological effects of each component. In drug development, they can create novel drugs with unique properties. The ability to tailor hybrid conjugates to specific applications makes them valuable tools for researchers and developers seeking innovative solutions to complex challenges.[21]

Recently, we reported the synthesis of 8-caffeinyl-triazolylmethoxy hybrid conjugates **3** (Fig. 4),[15] which are C8–O caffeine derivatives exhibiting significant anticancer properties. In pursuit of our ongoing research on synthesis and biological assessments of 8-caffeinyl-hybrid conjugate compounds,[22–24] hereby, we present our latest work on the synthesis, evaluation of anticancer activity, and *in silico* analysis of novel 8-caffeinyl chalcone hybrid conjugates, the general structures of which are illustrated in Fig. 5.

2. Results and discussion

2.1 Chemistry

For the synthesis of the title compounds, 8-BC was primarily synthesized using the standard procedure.[22] Subsequently, ketone **6** and/or aldehyde **7** were prepared by reacting 4-hydroxy acetophenone and/or 4-hydroxy benzaldehyde with 8-BC using K_2CO_3 as a base in anhydrous DMF (Scheme 1). An attempt was made to couple ketone **6** and/or aldehyde **7** with desired aromatic aldehydes and/or aromatic methylketones using NaOH as a base in EtOH (90%) under reflux conditions (Scheme 1). Contrary to our expectations, products **4** and/or **5** were not

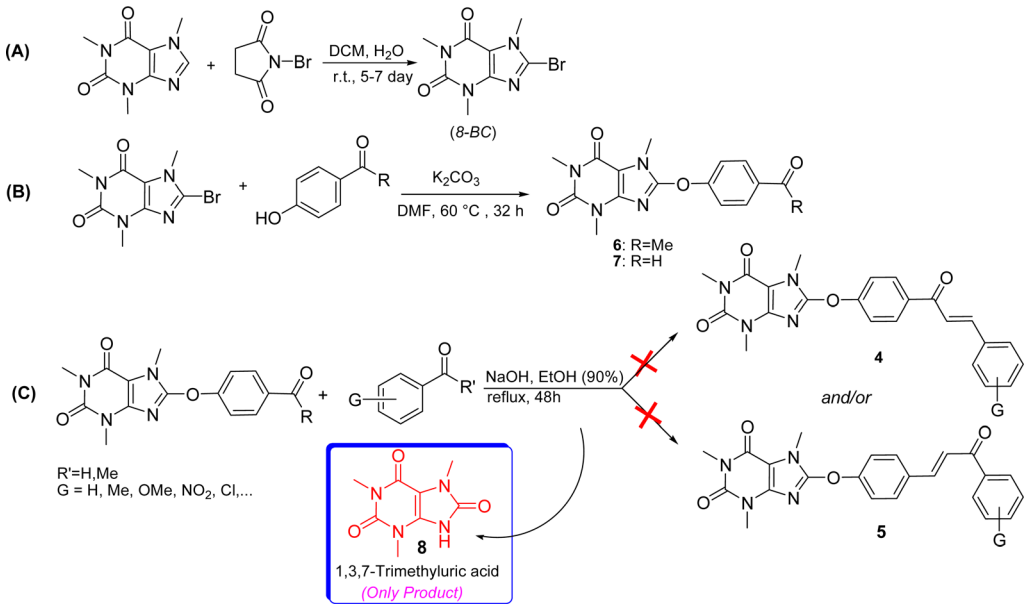

Scheme 1 Attempted synthesis of compounds **4** and **5** (A–C) along with the initial generation of 1,3,7-trimethyluric acid.

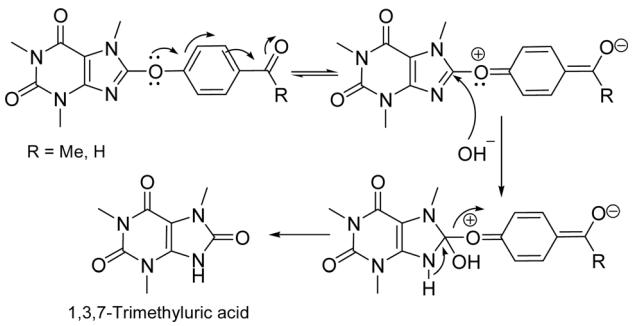

Scheme 2 A plausible mechanism for generation of 1,3,7-trimethyluric acid.

obtained. Surprisingly, only 1,3,7-trimethyluric acid (**8**) was obtained as a side product. The question arises: how is it possible? It is believed that due to the electron-withdrawing effect of the carbonyl group in both structures **6** and **7**, the charge density on the oxygen atom connected to the caffeinyl group is transferred to the carbonyl group through a mesomeric effect as shown in Scheme 2. This resonance effect leads to an increase in the positive charge density on C8, making it susceptible to attack by external nucleophiles such as OH^- through an S_NAr-type reaction, as illustrated in Scheme 2. After unsuccessful attempts to synthesize the desired compounds using the aforementioned procedure, the strategy was altered. Two sets of chalcone analogues, **9** and **10**, were initially prepared using either the standard Claisen–Schmidt[25] or acid-catalyzed aldol condensation methods,[26] respectively (Scheme 3). In this process, 4-hydroxyacetophenone and/or 4-hydroxybenzaldehyde were condensed with aromatic aldehydes and/or aromatic methylketones containing various functional groups, utilizing NaOH in EtOH (90%) under reflux conditions. After synthesizing chalcones **9** and **10**, they were combined with 8-BC using K_2CO_3 as a base in anhydrous DMF to produce the desired 8-caffeinyl chalcone hybrid conjugates **4a–4k** and **5a–5f**. These conjugates contained both electron-donating and/or electron-withdrawing groups and were obtained in good to excellent yields (Scheme 3).

2.2 *In vitro* anticancer and cytotoxic activity

The A-375 cell line is a well-known human melanoma cell line that originated from a tumor in a 54 year-old woman with malignant melanoma. This cell line is valuable for research in pharmacology, immuno-oncology, and toxicology.[27] The MCF-7 cell line, derived from a 69 year-old woman with breast adenocarcinoma in 1973, is among the most widely used human breast cancer cell lines globally. Researchers are drawn to the MCF-7 cell line due to its retention of characteristics resembling those of breast epithelium. It is frequently employed as an *in vitro* model for studying breast cancer biology. With its various subtypes, this cell line finds extensive applications in developing chemotherapeutic drugs and exploring drug resistance.[28] HEK-293, originating from human embryonic kidney cells in 1973, is a normal cell line commonly utilized in fundamental medical and pharmacological research.[29] The IC_{50} values pertaining to toxicity assessments of all synthetic products are outlined in Table 1.

Based on the MTT assay results, it was found that, with the exception of compounds **4f**, **4h**, and **5c–5e**, all other entries exhibited stronger anticancer activity compared to the reference drug MTX for the melanoma cancer cell line A375. Among these compounds, **4k** ($IC_{50} = 92 \pm 3.2$) showed the highest potency against the A375 cell line.

In Table 1, it is shown that for the breast cancer cell line MCF-7, the compounds demonstrated greater activity and potency compared to the A375 cell line. For example, compounds **4d** ($IC_{50} = 18 \pm 1.9$), **4e** ($IC_{50} = 35 \pm 2.2$), and **4k**

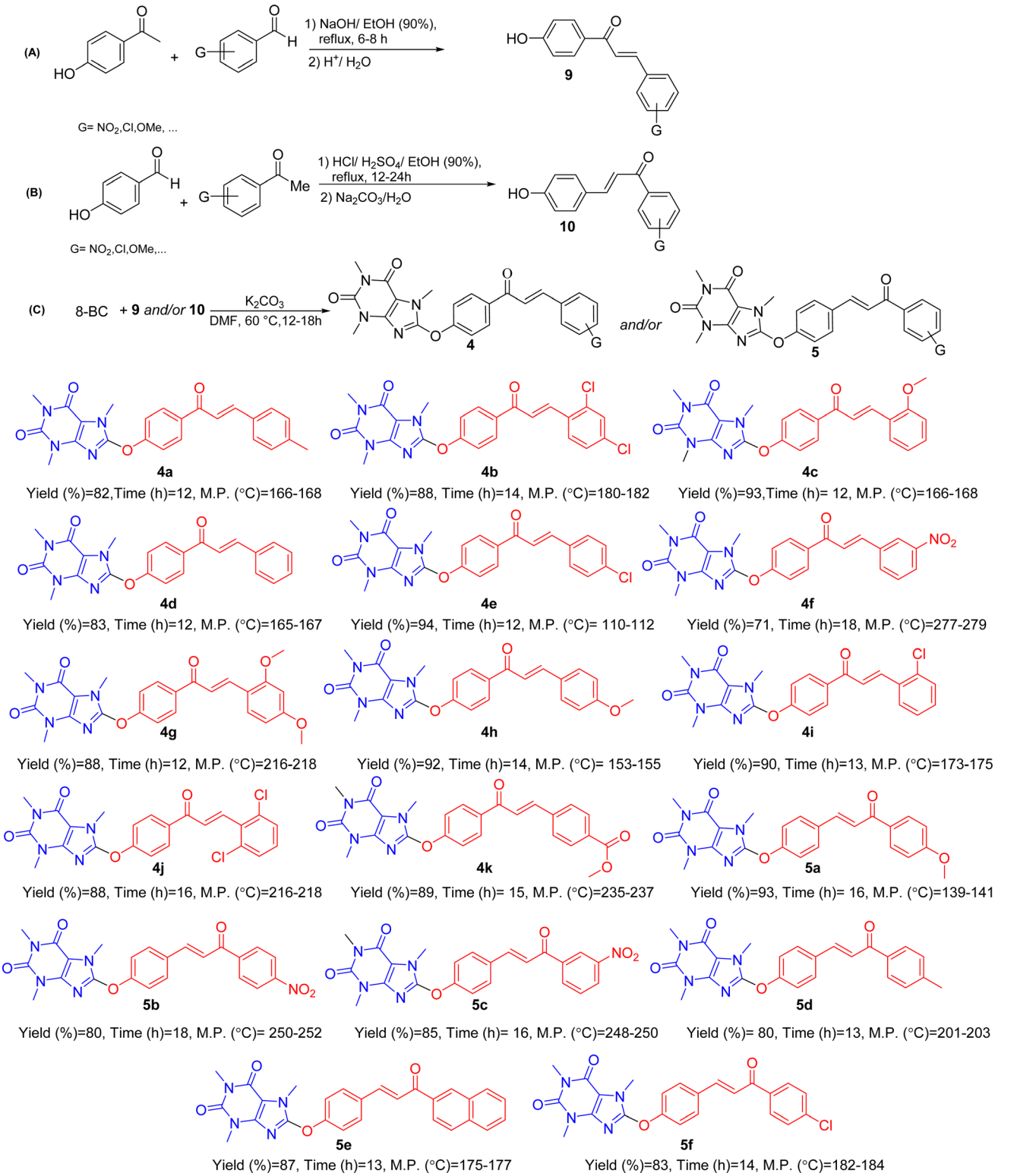

Scheme 3 General synthetic pathway (A–C) for preparing novel 8-caffeinyl chalcone hybrid conjugates and the structure of synthesized compounds.

($IC_{50} = 34 \pm 3.5$) were significantly more potent than MTX, with almost 19, 10, and 10 times greater efficacy, respectively. Except for compounds **4f–4h**, **5c**, and **5d**, all other tested compounds also outperformed MTX against MCF-7.

To assess the toxicity of the compounds, they were tested on the normal cell line HEK-293 (as shown in Table 1). Compounds **4f–4h**, **5a**, and **5c–5e** were found to be non-toxic to HEK-293 cells, while the remaining compounds, including MTX,

Table 1 The IC_{50} values (μM) of **4a–4k**, **5a–5f** and MTX against A-375, MCF7 and HEK-293 cell lines

Compound	A375	MCF-7	HEK-293
4a	279 ± 2.3	38 ± 3.7	407 ± 3.1
4b	325 ± 3.1	230 ± 3.2	347 ± 4.2
4c	325 ± 3.8	269 ± 4.5	451 ± 2.4
4d	157 ± 4.2	18 ± 1.9	220 ± 3.4
4e	273 ± 3.4	35 ± 2.2	386 ± 3.2
4f	>500	>500	>500
4g	425 ± 3.5	>500	>500
4h	>500	>500	>500
4i	111 ± 1.9	108 ± 3.1	162 ± 4.2
4j	200 ± 4.3	181 ± 3.1	214 ± 4.3
4k	92 ± 3.2	34 ± 3.5	99 ± 3
5a	249 ± 3.6	249 ± 3.2	>500
5b	275 ± 3.7	223 ± 3.7	419 ± 4.6
5c	>500	>500	>500
5d	>500	>500	>500
5e	>500	333 ± 2.5	>500
5f	368 ± 3.1	130 ± 3.4	240 ± 3.7
MTX	418 ± 2.0	343 ± 3.6	199 ± 2.4

exhibited varying degrees of toxicity. Among the compounds showing toxicity, **4a–4f**, **4j**, **5b**, and **5f** were less toxic than MTX, whereas **4i** and **4k** were more toxic. Notably, **4k** was identified as the most toxic compound, despite displaying the highest potency against all tested cancer cells.

The viability percentages of the examined cell lines at different concentrations (15.62, 31.25, 62.5, 125, 250, and 500 μM) of **4a–4k**, **5a–5f** and MTX are depicted in Fig. 6A–C. A *p*-value less than 0.05 (typically ≤0.05) indicates statistical significance, denoted by stars in Fig. 6A–C. Fig. 6A highlights that for A375, the lowest viability values and thus the highest toxicity are associated with **4i** and **4k** compared to all synthesized compounds at different concentrations. Furthermore, compounds **4a**, **4h**, and **5f** have shown lower viability and therefore higher toxicity compared to MTX. In the breast cancer cell line MCF-7 (Fig. 6B), **4k** was found to have the lowest viability rate compared to the other tested compounds and MTX. Additionally, **4a**, **4e**, **4g–4i**, **5d**, and **5f** were confirmed to exhibit lower viability than MTX, especially at lower concentrations. Overall, the majority of compounds demonstrated reduced viability to some extent at various concentrations. Compound **4f** was found to have the lowest toxicity compared to the other compounds tested. Fig. 6C displays the viability percentage of the normal cell line HEK-293. It is evident from the figure that **4k** exhibited the highest toxicity and lowest viability among all examined concentrations compared to the other synthesized compounds for HEK-293. Compounds **4i** and **5f** were found to be more toxic to HEK-293 compared to MTX, particularly at lower concentrations. Generally, MTX showed the highest toxicity against HEK-293 at 500 μM.

2.3 Plausible mechanism of anticancer activity and SAR analysis

Folic acid, also known as folacin, is a water-soluble vitamin categorized as vitamin B9. It plays a vital role in various biological processes, including the synthesis and modification of DNA and RNA, the production of methionine, and various chemical reactions within cellular metabolism. Folic acid serves as a precursor for the creation of tetrahydrofolate (coenzyme F) through the enzymatic activity of dihydrofolate reductase (DHFR).[30] Through a process involving one-carbon transfer metabolism and the enzymatic function of thymidylate synthase (TS), coenzyme F transfers a methyl group to deoxyuridine monophosphate (dUMP), converting it to deoxythymidine monophosphate (dTMP). This conversion is crucial for DNA synthesis and cell replication.[31] Inhibiting DHFR can halt the synthesis of coenzyme F, thereby disrupting DNA synthesis and related biochemical processes. Compounds like methotrexate (MTX) and aminopterin share a structural resemblance to folic acid, comprising three molecular components: pteridine, *p*-aminobenzoic acid (PABA), and glutamic acid. The primary difference lies in the pteridine core, which is responsible for DHFR inhibition.[32] The pteridine core, a key pharmacophoric site in folic acid, MTX, and aminopterin, bears a striking resemblance to xanthine alkaloids. As shown in Fig. 7, the compounds have similarities to folic acid, MTX, and aminopterin. In this regard, the caffeinyl moiety can be considered as a successor of pteridine, while part of chalcone in compound **4** series act as PABA's pharmacophores exist in folic acid and its derivatives. Other part of compound **4** series comprising double bond, aromatic ring "B" and its substituents can be consider as a glutamate residue. In particular, **4k** involving hydrolyzable ester moiety in para position is the most potent compound that mimics glutamate residue in folic acid and its antimetabolic derivatives. In general, compound **4** series displayed more reactivity than compound **5** series which can be attributed to more structural resemblance of compound **4** series to folate analogues compare to **5**.

Although there is no apparent trend in the SAR of the title compounds, some insights can be gleaned from the types of substituents in both the compound **4** and **5** series. Generally, the presence of mono chloro or dichloro atoms in both series **4** and **5** led to anticancer activity, as seen in **4b**, **4e**, **4i**, **4j**, and **5f**. The presence of electron-releasing groups like methoxy, either as a mono or di-substituent, produced varying results in both series **4** and **5**. While **4c** and **5a** exhibited anticancer activity, **4g** and **4h** did not. Similarly, the presence of nitro as an electron-withdrawing moiety had differing outcomes. Compound **5b** showed anticancer activity, while **4f** and **5c** did not. Similarly, the presence of methyl in **4a** confirmed anticancer activity but resulted in the opposite outcome in **5d** under the same conditions.

2.4 *In silico* studies

2.4.1 Docking study. The strong anti-cancer properties of compounds **4k** and **5a** against the melanoma A375 cell line led us to explore how they might interact with the active site of B-RAF kinase, a target enzyme. The most common oncogenic mutation of B-RAF is the substitution of Val600 with Glu in the B-RAF V600E mutation.[33] To investigate this, we utilized Molegro Virtual Docker (MVD 6.0) with default settings to study the

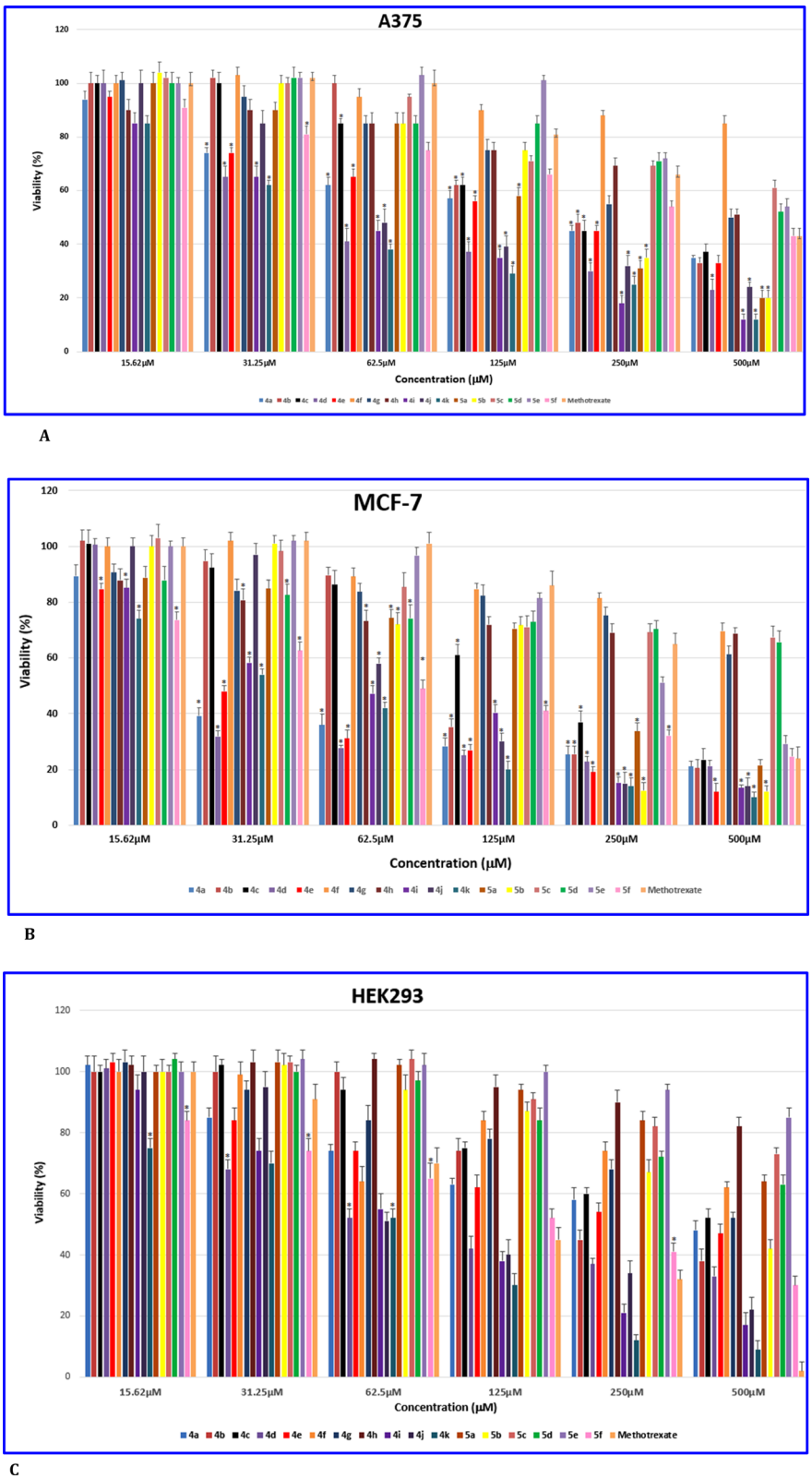

Fig. 6 (A) The viability assessment for **4a–4k**, **5a–5f** and MTX against A375. (B) The viability assessment for **4a–4k**, **5a–5f** and MTX against MCF-7. (C) The viability assessment for **4a–4k**, **5a–5f** and MTX against HEK293.

potential interactions and binding modes of **4k** and **5a** in the active site of B-RAF V600E.[34] The three-dimensional crystal structure of B-RAF V600E (PDB code: 3OG7) complexed with vemurafenib (PLX4032) was retrieved from the protein data bank (RSCB), and the docking results were analyzed using Discovery Studio 2021 software. The validity of the docking

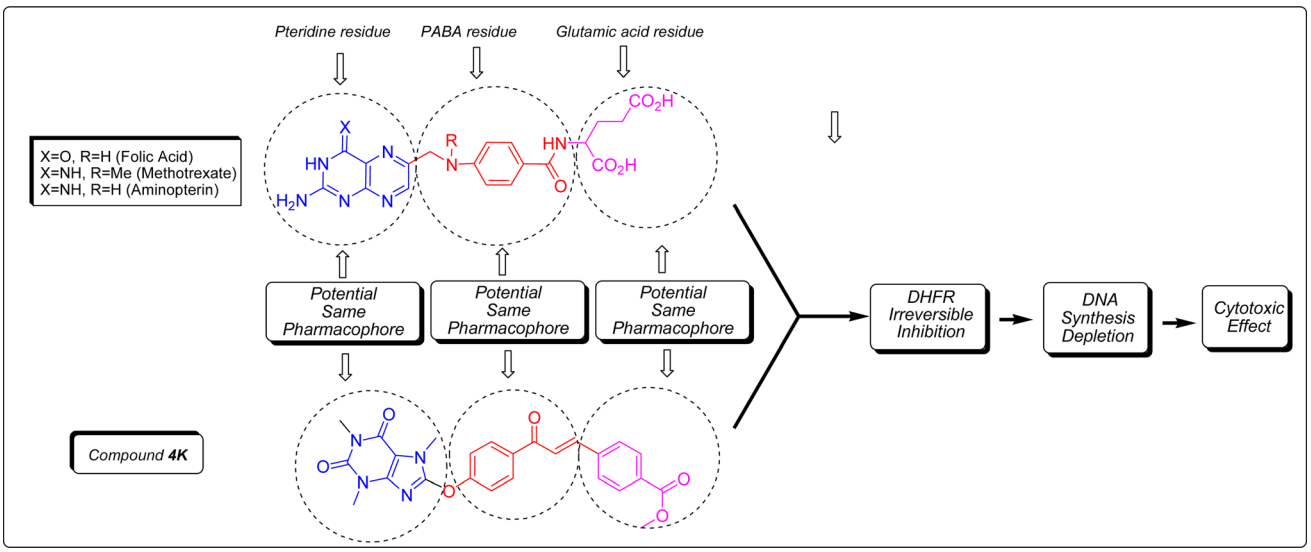

Fig. 7 The possible anticancer mechanism of 8-caffeinyl chalcone hybrid conjugates.

process was confirmed by redocking vemurafenib into the enzyme's active site, resulting in a root-mean-square deviation (RMSD) value of 1.72 Å compared to the co-crystallized structure. This RMSD value, below 2 Å, is considered acceptable for validating the docking protocol.[35] Thus, the methodology employed was deemed suitable for conducting docking studies of **4k** and **5a** in the enzyme's active site.

The significant interactions for stabilization of vemurafenib in the active site of B-RAF V600E kinase enzyme include van der Waals, hydrophobic, π–alkyl, π–π stack, π–sigma, π–cation, and hydrogen bond interactions. The π–π stacking interactions of the heterocyclic ring of vemurafenib were created with Trp531 and Phe583. Six conventional hydrogen bonds were observed between vemurafenib and the residues of Lys483, Gln530, Cys532, Asp594, Phe595, and Gly596. Additionally, one carbon–hydrogen bond was detected between vemurafenib and the residue of Cys532. The side chain of Ala481 and Cys532 was participated in π–alkyl interaction with the heterocyclic ring of vemurafenib. The hydrophobic and van der Waals interactions of vemurafenib were detected with the side chains of Ile463, Val471, Leu505, Ile513, Leu515, Phe516, Ile527, Val528, Thr529, Gly534, Ser535, Ser536, His539, Lys591, and Gly593. The heterocyclic ring of vemurafenib was participated in a π–sigma interaction with Leu514. Also, a π–cation interaction was detected between the residue of Lys483 and the phenyl ring of vemurafenib. The docked conformation of vemurafenib including hydrogen bond interactions and the overlay view of conformations of co-crystallized vemurafenib, re-docked vemurafenib, **4k** and **5a** in the active site of an enzyme are depicted in Fig. 8. Delightfully, **4k** and **5a** bind to the identical site similar to vemurafenib and exhibits robust interactions with the B-RAF V600E enzyme as illustrated in Fig. 8.

The docked conformations of **4k** in active site of B-RAF V600E kinase including hydrogen bond interactions is presented in Fig. 9. For **4k**, the analysis of the docking protocol revealed that Thr529 is participated in a π–sigma interaction with phenoxy residue. Both rings of caffeine core are involved in π–π interactions with Phe583. Four conventional hydrogen

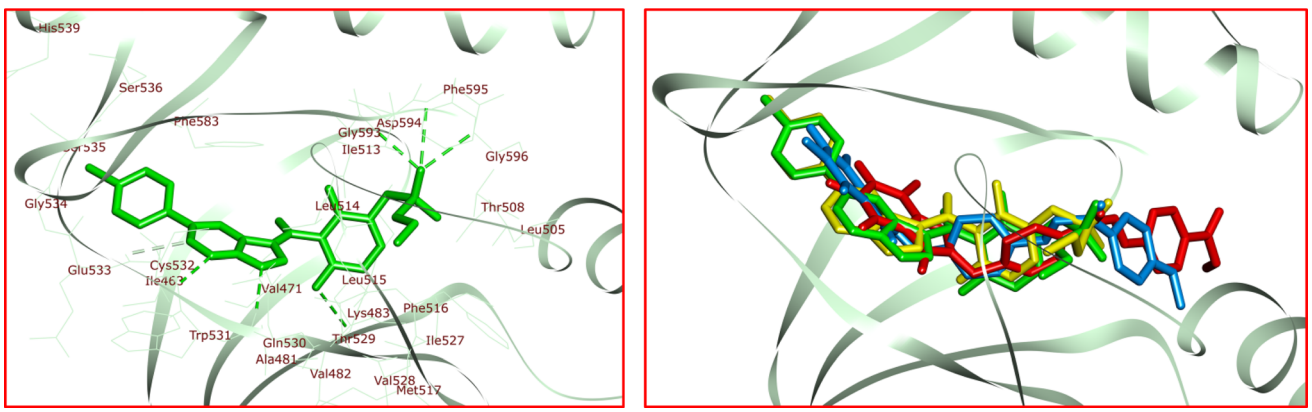

Fig. 8 Docked conformation of vemurafenib including hydrogen bond interactions [left] and the overlay view of conformations of co-crystallized vemurafenib (yellow), re-docked vemurafenib (green), **4k** (red) and **5a** (blue) [right] in active site of B-RAF V600E kinase.

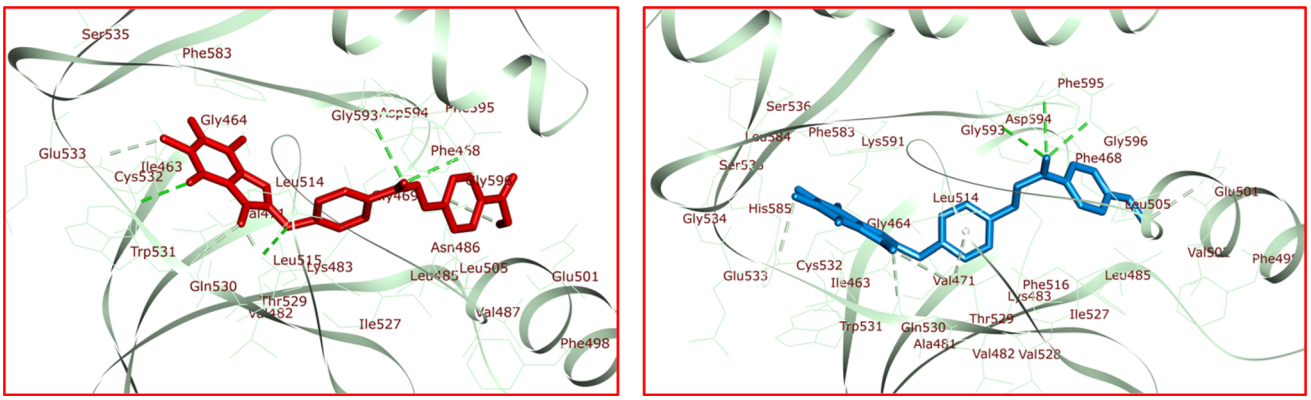

Fig. 9 Docked conformations of **4k** (left) and **5a** (right) including hydrogen bond interactions in the active site of B-RAF V600E kinase.

bonds were detected between **4k** and the residues of Thr529, Cys532, Asp594, and Gly596. In addition, several carbon–hydrogen bonds were observed between **4k** and the side chain of Phe468, Thr529, Gln530, and Cys532. The residue of Val471, Ala481, Leu514, Cys532, and Phe583 was involved in π–alkyl interactions with the caffeine core of **4k**. The two phenyl rings of **4k** were involved in additional π–alkyl interactions with the side chain of Lys483, Leu485, Leu514, and Ile527. The hydrophobic and van der Waals interactions of **4k** are similar to those observed for vemurafenib since both compounds were placed in the same binding pocket.

The interactions that play a significant role in stabilizing vemurafenib within the active site of the B-RAF V600E kinase enzyme consist of van der Waals, hydrophobic, π–alkyl, π–π stacking, π–sigma, π–cation, and hydrogen bond interactions. Specifically, the π–π stacking interactions between the heterocyclic ring of vemurafenib and Trp531 and Phe583 were identified. A total of six conventional hydrogen bonds were also noted between vemurafenib and the amino acid residues Lys483, Gln530, Cys532, Asp594, Phe595, and Gly596. Additionally, a carbon–hydrogen bond was observed between vemurafenib and the residue Cys532. The side chains of Ala481 and Cys532 were involved in π–alkyl interactions with the heterocyclic ring of vemurafenib. Furthermore, the hydrophobic and van der Waals interactions of vemurafenib were found to interact with the side chains of Ile463, Val471, Leu505, Ile513, Leu515, Phe516, Ile527, Val528, Thr529, Gly534, Ser535, Ser536, His539, Lys591, and Gly593. The heterocyclic ring of vemurafenib engaged in a π–sigma interaction with Leu514, while a π–cation interaction was observed between Lys483 and the phenyl ring of vemurafenib. The docked conformation of vemurafenib, along with its hydrogen bond interactions, and comparative conformations with other compounds in the active site of the enzyme are depicted in Fig. 8.

Similarly, the docked conformations of **4k** within the active site of the B-RAF V600E kinase, including its hydrogen bond interactions, are presented in Fig. 9. Analysis of the docking process for **4k** indicated a π–sigma interaction between Thr529 and the phenoxy residue. Both rings of the caffeine core of **4k** participated in π–π interactions with Phe583. Four conventional hydrogen bonds were identified between **4k** and the residues Thr529, Cys532, Asp594, and Gly596. Additionally, several carbon–hydrogen bonds were observed between **4k** and the side chains of Phe468, Thr529, Gln530, and Cys532. The residues Val471, Ala481, Leu514, Cys532, and Phe583 were involved in π–alkyl interactions with the caffeine core of **4k**. Moreover, the two phenyl rings of **4k** engaged in additional π–alkyl interactions with the side chains of Lys483, Leu485, Leu514, and Ile527. The hydrophobic and van der Waals interactions of **4k** were similar to those observed for vemurafenib, given that both compounds occupy the same binding pocket.

The residue from **5a** known as anisole engaged in a π–cation interaction with Lys483 (Fig. 9). In addition, it participated in a π–sigma interaction with Gly596. Cys532 formed two π–sulfur interactions with both rings of the caffeine core. Two π–π interactions were observed between the caffeine core of **5a** and Phe583. Furthermore, **5a** interacted with Thr529 through both π–donor and carbon–hydrogen bonds. Additionally, Glu501, Thr529, Gln530, and Cys532 contributed to other carbon–hydrogen bond interactions with **5a**. Three conventional hydrogen bond interactions were noted between **5a** and the residues Asp594, Phe595, and Gly596. **5a** was also stabilized in the active site of the target enzyme through π–alkyl interactions with the side chains of Val471, Ala481, Phe498, Leu505, Leu514, Ile527, and Phe583. The hydrophobic and van der Waals interactions of **5a** showed similarity to those observed for vemurafenib and **4k**. The calculated ΔG values for vemurafenib, **4k**, and **5a** were −154.54, −159.56, and −151.35 kcal mol^{-1}, respectively. The total hydrogen bond energies for vemurafenib, **4k**, and **5a** were −11.13, −10.90, and −6.13 (kcal mol^{-1}), respectively. These findings suggest that hydrogen bonds, hydrophobic, and van der Waals interactions play a crucial role in stabilizing **4k** and **5a** in the binding site of the B-RAF V600E kinase enzyme.

Dihydrofolate reductase (DHFR) is essential for folic acid metabolism and the production of purines, thymidylate, and glycine.[36] DHFR is a key target for cancer treatment. In this study, the interaction, affinity, binding mode, and orientation of compounds **4k** and **5a** were investigated in the active site of human DHFR using MVD 6.0 software. The 3D structure of

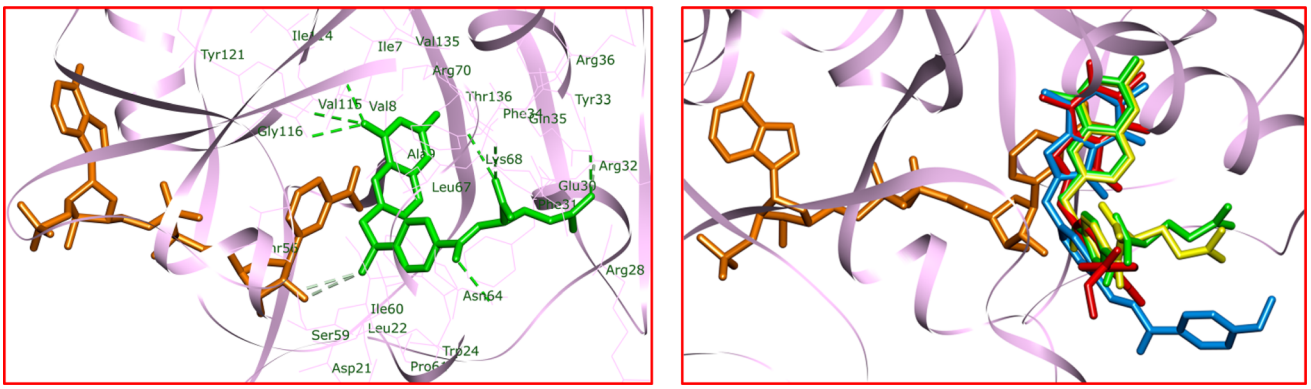

Fig. 10 Docked conformation of MTX including hydrogen bond interactions [left] and the overlay view of conformations of co-crystallized MTX (yellow), re-docked MTX (green), **4k** (red) and **5a** (blue) [right] in active site of hDHFR.

human DHFR in complex with methotrexate (MTX) and nicotinamide adenine dinucleotide phosphate (NADPH) was obtained from the RCSB (PDB code: 1U72). Discovery Studio 2021 software was used for the analysis of results. The docking protocol was validated by redocking MTX in the active site of hDHFR, with a desirable RMSD value of 1.18 Å. Analysis revealed that hydrogen bond interactions are crucial for the stabilization of MTX in the active site. Strong hydrogen bonds were identified between MTX and Ile7, Gln35, Asn64, Arg70, Val115, and Tyr121 residues. NADPH, Arg32, and Ser59 formed carbon–hydrogen bond interactions with MTX. Additionally, Ile7, Ala9, Leu22, and NADPH participated in π–alkyl interactions with the pteridine core of MTX. A π–alkyl interaction was observed between Ile60 and the aryl ring of MTX. Hydrophobic and van der Waals interactions of MTX were detected in a pocket formed by Ile7, Val8, Leu22, TRP24, Phe31, Tyr33, F34, Gln35, Thr38, Thr39, Ser59, Pro61, Leu67, Lys68, Val115, Gly116, Val135, and Phe179. The binding of **4k**, **5a**, and MTX to the same site in hDHFR with strong interactions is depicted in Fig. 10.

In Fig. 11, the docked conformation of **4k** in the active site of hDHFR, along with its hydrogen bond interactions, is depicted. The ester group of **4k** formed two traditional hydrogen bonds with Lys68 and Arg70. Additionally, it engaged in two carbon–hydrogen bond interactions with Asn64 and Lys68. The central caffeine core of **4k** participated in multiple carbon–hydrogen bond interactions with the side chains of Ile7, Glu30, Val115, Tyr121, and Thr136. Furthermore, π–π shaped and π–amide stacked interactions were observed between **4k** and Phe34 and Val8, respectively. **4k** also interacted through π–alkyl interactions with Ala9, Phe31, Fhe34, Ile60, and NADPH. The van der Waals and hydrophobic interactions of **4k** in the binding site were similar to those of MTX.

On the other hand, in the case of **5a** (Fig. 11), there were no conventional hydrogen bond interactions observed. The caffeine core of **5a** engaged in four carbon–hydrogen bond interactions with Ile7, Glu30, Val115, and Tyr121. Additionally, a π–donor hydrogen bond formed between Ser59 and the phenoxy ring of **5a**. Similar to **4k**, π–π shaped and π–amide stacked interactions were detected between **5a** and Phe34 and Val8, respectively. The caffeine core of **5a** also participated in four π–alkyl interactions with Ala9, Phe34, and NADPH. Other parts of the **5a** structure exhibited several π–alkyl interactions with the side chains of Leu22, Pro26, Phe31, Ile60, and Pro61. The hydrophobic and van der Waals interactions of **5a** mirrored

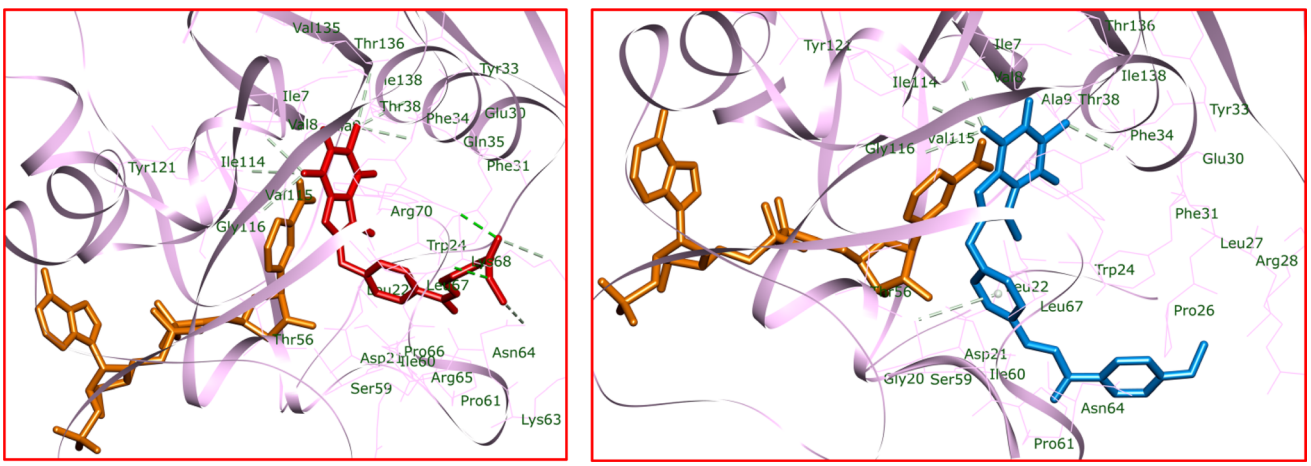

Fig. 11 Docked conformations of **4k** (left) and **5a** (right) including hydrogen bond interactions in the active site of hDHFR.

those observed for MTX and **4k**. Calculated ΔG values for MTX, **4k**, and **5a** were −190.40, −177.89, and −163.62 kcal mol^{-1}, respectively. The total hydrogen bond energies for MTX, **4k**, and **5a** were −16.33, −4.56, and −7.02 (kcal mol^{-1}), respectively. The docking study results suggest that the stabilization of MTX, **4k**, and **5a** in the hDHFR enzyme's binding site may be facilitated by strong hydrogen bonds, hydrophobic interactions, and van der Waals forces. The presence of NADPH could also impact the stabilization of ligands in the active site of the enzyme.

2.4.2 *In silico* physiochemical and pharmacokinetic profile studies. The physiochemical parameters of a drug candidate are often determined based on Lipinski's rule of five (RO5). This rule assesses molecular characteristics such as molecular weight, number of rotatable bonds, hydrogen bond donors and acceptors, and the octanol–water partition coefficient (log *P*) to predict the likelihood of a compound being suitable as a drug.[37,38] In the evaluation of drug candidates **4a–4k**, **5a–5f**, and MTX, *in silico* pharmacokinetic and physiochemical profiles were analyzed using tools like the preADMET online server,[39] OSIRIS Property Explorer,[40] and the SwissADME online software,[41] with the results summarized in Tables 2 and 3.

From the data presented in Table 2, it can be observed that both MTX and the synthesized compounds adhere to the molecular weight criterion of ≤500 dalton. The number of rotatable bonds (*n*RB) for MTX and the synthesized compounds falls within the 5–10 range. Additionally, all compounds meet the criteria for hydrogen bond acceptors (*n*HBA), hydrogen bond donors (*n*HBD), and the lipophilicity factor indicated by *c* log *P*, with values below the specified threshold of 5 as per RO5 criteria.

The total polar surface area (TPSA) is an important parameter in determining a molecule's transport characteristics, influencing factors like intestinal absorption and blood–brain barrier penetration. TPSA values for **4a–4k** and **5a–5f** are below the accepted limit of 140 Å^2 for approved drugs, suggesting favorable membrane permeability or oral absorption. The drug likeness of the synthesized derivatives was evaluated using the OSIRIS Property Explorer software, indicating negative values for compounds **4f**, **4k**, **5b**, and **5c**, along with MTX.

These analyses led to the computation of a drug score for each compound, serving as a predictive parameter. The maximum drug score values were observed for compounds **4c** and **5a**, while the minimum scores belonged to compounds **4h** and **5b**. Overall, the drug score values for the synthesized compounds surpass that of MTX across the board. Notably, compounds **4k** and **5a** exhibit promising potential for further research based on these assessments.

The pharmacokinetic profiles of compounds **4a–4k**, **5a–5f**, and MTX, including their absorption, distribution, metabolism, and toxicity properties, were measured and summarized in Table 3. The analysis focused on assessing these compounds as *P*-glycoprotein (*P*-gp) substrates and/or inhibitors, their human intestinal absorption (HIA), aqueous solubility (log *S*), and skin permeability (log K_p) to predict their absorption profiles. Most of the synthesized compounds exhibited moderate solubility in water, while methotrexate (MTX) showed good water solubility. The HIA factor was found to be over 96.49% for **4a–4k** and **5a–5f**, in contrast to 36.61% for MTX, suggesting ideal intestinal absorption for the former compounds. Skin permeability, crucial for transdermal drug delivery, was comparable among **4a–4k**, **5a–5f**, and MTX. The compounds were also evaluated for their interaction with the *P*-gp transporter, which plays a role in drug bioavailability. While all synthesized compounds were found to be non-substrates of *P*-gp, MTX was predicted to be a substrate; however, it is not an inhibitor. The synthesized compounds were also assessed for their blood–brain barrier (BBB) permeability, with all compounds except **5e** showing low permeability, suggesting minimal risk of neurotoxicity.

Table 2 Physicochemical properties of **4a–4k**, **5a–5f**, and methotrexate

Compound	Mw[a]	*n*RB[b]	*n*HBD[c]	*n*HBA[d]	clog *P*[e]	TPSA[f]	Drug-likeness	Drug score
4a	430.46	5	0	5	3.57	88.12	2.53	0.45
4b	485.32	5	0	5	4.44	88.12	4.94	0.34
4c	446.46	6	0	6	3.16	97.35	4.42	0.49
4d	416.43	5	0	5	3.23	88.12	0.95	0.44
4e	450.87	5	0	5	3.84	88.12	4.59	0.42
4f	461.43	6	0	7	2.31	133.94	−1.05	0.29
4g	476.48	7	0	7	3.09	106.58	3.01	0.46
4h	446.46	6	0	6	3.16	97.35	3.96	0.23
4i	450.87	5	0	5	3.84	88.12	4.57	0.25
4j	485.32	5	0	5	4.44	88.12	4.45	0.34
4k	474.47	7	0	7	3.14	114.42	−2.15	0.25
5a	446.46	6	0	6	3.16	97.35	3.85	0.49
5b	461.43	6	0	7	2.31	133.94	−8.10	0.23
5c	461.43	6	0	7	2.31	133.94	−2.71	0.25
5d	430.46	5	0	5	3.57	88.12	2.95	0.46
5e	466.49	5	0	5	4.43	88.12	1.17	0.31
5f	450.87	5	0	5	3.84	88.12	5.42	0.42
MTX[g]	454.44	10	5	9	1.23	210.54	−7.09	0.22

[a] Molecular weight. [b] Number of rotatable bonds. [c] Number of hydrogen bond donors. [d] Number of hydrogen bond acceptors. [e] Logarithm of octanol–water partition coefficient (log *P*). [f] Topological polar surface area (Å^2). [g] Methotrexate.

Table 3 Pharmacokinetic profile of **4a–4k**, **5a–5f**, and methotrexate

Compound	log *S*	HIA[a]	log K_p[b]	*P*-gp[c]	BBB[d]	CYP2D6	CYP3A4	Carcino.[e]	hERG inhibition[f]
4a	−4.91	98.69	−3.06	I/NS	0.29	NI/NS	NI/NS	NC	Medium
4b	−5.79	97.65	−3.08	I/NS	0.49	NI/NS	NI/WS	NC	Medium
4c	−4.68	99.39	−3.24	I/NS	0.40	NI/NS	NI/NS	NC	Medium
4d	−4.61	98.85	−3.07	I/NS	0.27	NI/NS	NI/WS	NC	Medium
4e	−5.20	98.07	−3.13	I/NS	0.33	NI/NS	NI/WS	NC	Medium
4f	−4.67	97.43	−2.90	I/NS	0.22	NI/NS	NI/WS	C	Medium
4g	−4.75	99.73	−3.48	I/NS	0.41	NI/NS	NI/WS	NC	Medium
4h	−4.68	99.39	−3.27	I/NS	0.40	NI/NS	NI/NS	NC	Medium
4i	−5.20	98.07	−3.10	I/NS	0.32	NI/NS	NI/WS	NC	Medium
4j	−5.20	97.65	−3.06	I/NS	0.47	NI/NS	NI/WS	NC	Medium
4k	−4.69	99.65	−3.27	I/NS	0.32	NI/NS	NI/NS	NC	Medium
5a	−4.68	99.29	−3.30	I/NS	0.50	NI/NS	NI/NS	NC	Medium
5b	−4.67	97.43	−2.90	I/NS	0.19	NI/NS	NI/WS	C	Medium
5c	−4.67	96.49	−2.87	I/NS	0.25	NI/NS	NI/WS	C	Medium
5d	−4.91	98.50	−3.09	I/NS	0.55	NI/NS	NI/NS	NC	Medium
5e	−5.73	97.64	−2.80	I/NS	1.12	NI/NS	NI/WS	NC	Medium
5f	−5.20	98.07	−3.13	I/NS	0.56	NI/NS	NI/WS	NC	Medium
MTX[g]	−1.19	36.61	−4.63	NI/S	0.04	NI/NS	I/WS	NC	High

[a] Human intestinal absorption (%). [b] Skin permeability (log K_p, cm h^{-1}). [c] *P*-Glycoprotein. [d] Blood–brain barrier permeability (C. brain/C. blood). [e] Carcinogenicity (mouse). [f] Human ether-a-go-go related gene channel. [g] Methotrexate. S = substrate, WS = weak-substrate, NS = non-substrate, I = inhibitor, NI = non-inhibitor, NC = non-carcinogenic.

Regarding metabolism, the compounds were found to interact differently with the CYP2D6 and CYP3A4 enzymes. While they were mostly non-inhibitors and non-substrates of CYP2D6, some were substrates of CYP3A4, implicating potential liver metabolism. In terms of carcinogenicity, most compounds were deemed non-carcinogenic in mice. The risk of hERG inhibition, which can lead to cardiac side effects, was found to be high for MTX and moderate for **4a–4k** and **5a–5f**.

2.4.3 DFT study. To rationalize the plausible mechanism illustrated in Scheme 2, the molecular structures of compounds **6**, **7**, and 8-BC were studied using DFT-D3 methods to simulate them theoretically at the M06-2X-D3/6-31+G(d,p) level in the presence of either a 90% ethanol or DMF solvent. To provide a more precise description of van der Waals interactions, the dispersion correction developed by Grimme[42] was applied. The PCM solvent model was utilized for 90% ethanol (for

Table 4 The selected significant charge transfer between atoms in compounds **6** (R=Me) and **7** (R=H)

Pairwise charge transfer[a]	$E^{(2)}$, **7**	$E^{(2)}$, **6**	Pairwise charge transfer[b]	$E^{(2)}$, **7**	$E^{(2)}$, **6**	$E^{(2)}$, 8-BC
$n' O_{15} \rightarrow \sigma^* N_7–C_8$	1	55	$n N_1 \rightarrow \pi^* C_6–O_{13}$	70	70	72
$n O_{15} \rightarrow \sigma^* C_8–N_9$	10	10	$n N_1 \rightarrow \pi^* C_2–O_{11}$	70	69	70
$n' O_{15} \rightarrow \sigma^* C_8–N_9$	47	—	$n N_3 \rightarrow \sigma^* C_4–C_5$	—	60	59
$n N_9 \rightarrow \sigma^* C_8–O_{15}$	4	4	$n N_3 \rightarrow \sigma^* C_2–O_{11}$	—	74	77
$n' O_{15} \rightarrow \pi^* C_{25}–C_{26}$	22	19	$n N_9 \rightarrow \pi^* C_4–C_5$	—	92	96
$n O_{15} \rightarrow \sigma^* C_{25}–C_{30}$	8	5	$n N_9 \rightarrow \pi^* N_7–C_8$	—	197	213
$n O_{32} \rightarrow \sigma^* C_{31}–C_{37}$	—	23	$n N_9 \rightarrow \sigma^* C_7–C_8$	11	11	10
$n O_{32} \rightarrow \sigma^* C_{31}–H_{37}$	24	—	$n O_{11} \rightarrow \sigma^* C_2–N_1$	34	33	33
$n O_{32} \rightarrow \sigma^* C_{28}–C_{31}$	23	24	$n O_{11} \rightarrow \sigma^* C_2–N_3$	32	32	31
$\sigma C_4–N_9 \rightarrow \sigma^* C_8–O_{15}$	10	10	$n O_{13} \rightarrow \sigma^* N_1–C_6$	36	36	35
$\sigma C_5–N_7 \rightarrow \sigma^* C_8–O_{15}$	6	6	$n O_{13} \rightarrow \sigma^* C_5–C_6$	22	22	22
$\pi C_{25}–C_{26} \rightarrow \pi^* C_{29}–C_{30}$	24	24	$n O_{11} \rightarrow RY C_2$	13	13	5
$\pi C_{29}–C_{30} \rightarrow \pi^* C_{25}–C_{26}$	33	33	$n O_{13} \rightarrow RY C_6$	12	12	4
$\pi C_{25}–C_{26} \rightarrow \pi^* C_{27}–C_{28}$	32	32	$n Br_{15} \rightarrow \sigma^* N_7–C_8$	—	—	29
$\pi C_{27}–C_{28} \rightarrow \pi^* C_{25}–C_{26}$	25	26	$\pi C_4–C_5 \rightarrow \pi^* N_7–C_8$	—	15	20
$\pi C_{27}–C_{28} \rightarrow \pi^* C_{31}–O_{32}$	27	24	$\sigma C_4–C_5 \rightarrow \pi^* C_6–O_{13}$	—	40	38
$\pi C_{31}–O_{32} \rightarrow \pi^* C_{27}–C_{28}$	6	6	$\pi C_5–N_7 \rightarrow \pi^* N_3–C_4$	24	4	3
$\pi C_{27}–C_{28} \rightarrow \pi^* C_{29}–C_{30}$	30	30	$\pi C_5–N_7 \rightarrow \pi^* C_8–N_9$	51	2	1
$\pi C_{29}–C_{30} \rightarrow \pi^* C_{27}–C_{28}$	25	25	$\pi N_7–C_8 \rightarrow \pi^* C_4–C_5$	—	19	19
$\sigma C_{37}–H_{37} \rightarrow \sigma^* C_{31}–O_{32}$	—	12	$\sigma C_8–N_9 \rightarrow \sigma^* N_3–C_4$	64	8	8

[a] Pairwise charge transfer and stabilization energy $E^{(2)}$ (kcal mol^{-1}) for **6** and **7** in ethanol 90%. [b] Pairwise charge transfer and stabilization energy $E^{(2)}$ (kcal mol^{-1}) for **6**, **7** and 8-BC in DMF.

compounds **6** and **7**) and DMF (for 8-BC) solvents. Additionally, frequency calculations were conducted to confirm the stability of the optimized structures and verify the absence of imaginary frequencies.

2.4.3.1 NBO analysis. In the solution phase, second-order perturbation theory is employed to calculate the stabilization energy $E_{ij}^{(2)}$, for compounds **6**, **7**, and 8-BC. The donor–acceptor NBO stabilization energy is interpreted as follows:

$$E_{ij}^{(2)} = \frac{q_i \times F(i,j)^2}{E_i - E_j} \quad (1)$$

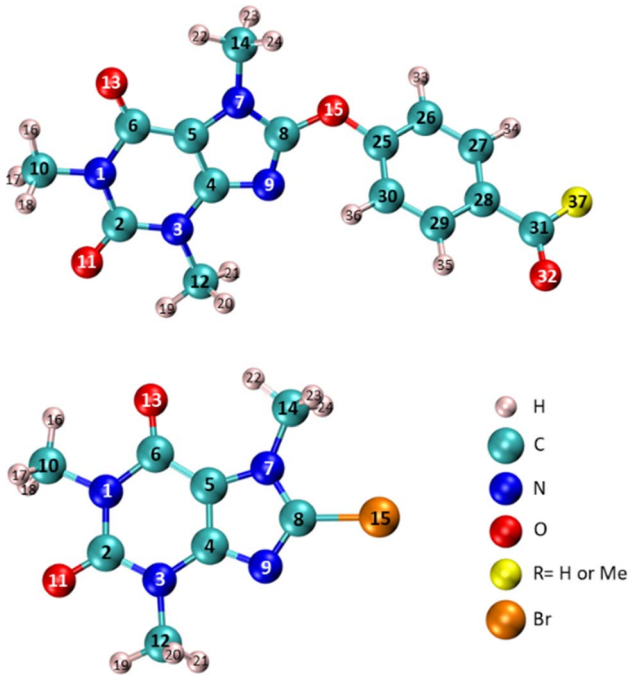

Fig. 12 Specification the atom number of compounds **6** (R=Me), **7** (R=H), and 8-BC used in Table 4.

where q_i represents the orbital occupancy of the donor, $F(i,j)$ denotes the off-diagonal NBO Fock matrix element, and E_i and E_j refer to the orbital energy of the diagonal elements. The $E^{(2)}$ energies of the notable donor–acceptor interionic NBO interactions within the 4-carbonylphenoxy residue of the molecules are detailed in Table 4. The atom numbering referenced in this table corresponds to that depicted in Fig. 12.

Table 4 illustrates that the n* NBO of O15 in compounds **6** and **7** displays a more pronounced donor character compared to the corresponding donor role of Br in 8-BC. Additionally, the charge transfer from the lone-pair electrons of O15 in compound **7** to the σ* orbital of C_{25}–C_{26}/C_{25}–C_{30} (two neighboring C–C bonds) differs slightly from the process observed in compound **6** because of difference in substituent at C28. The significant charge transfers between O15 and the caffeinyl moiety in the molecules originate from the strong interaction between O15 and the caffeinyl moiety. Furthermore, the charge transfer pathway from the atoms surrounding O15 towards the 4-carbonylphenoxy residue signifies an electron flow from the caffeinyl residue of compounds **6** and **7** towards the 4-carbonylphenoxy residue. Hence the charge density is transferred from caffeinyl residue toward 4-carbonylphenoxy group which causes the enhancement of positive charge density on caffeine's C8 and makes it suitable for susceptible attack by a nucleophile like hydroxide ion. These findings support the proposed mechanism depicted in Scheme 2 and are consistent with the experimental observations.

The natural atomic charge is determined by subtracting the nuclear charge from the total natural population of natural atomic orbitals within the atom. The natural atomic charge, referred to as the NBO charge in Fig. 13, is obtained through NBO analysis. Additionally, Fig. 13 illustrates the CHelpG atomic charge derived from Breneman atomic radii, and the ESP atomic charge based on Merz–Kollman atomic radii. In Fig. 13, the atomic charges (NBO, CHelpG, or ESP) of

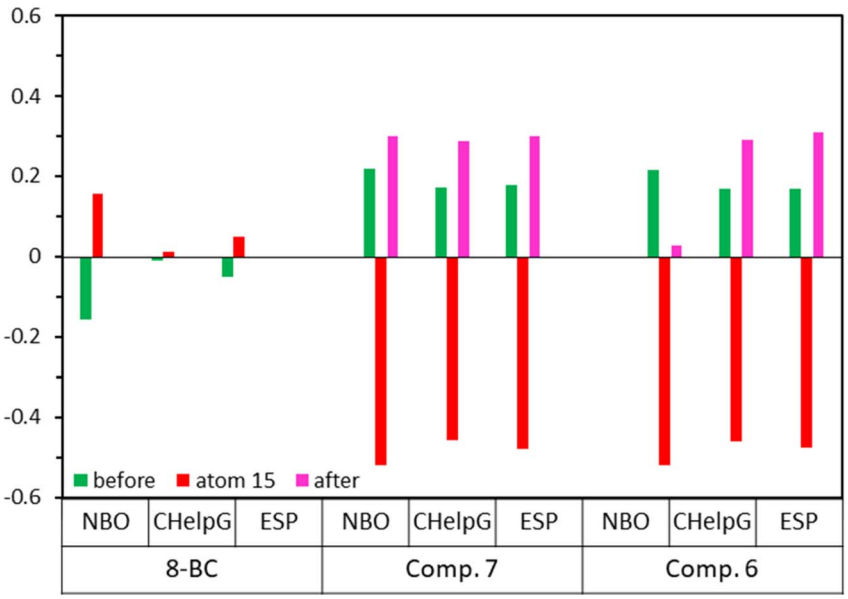

Fig. 13 Charge distribution on three parts of molecules.

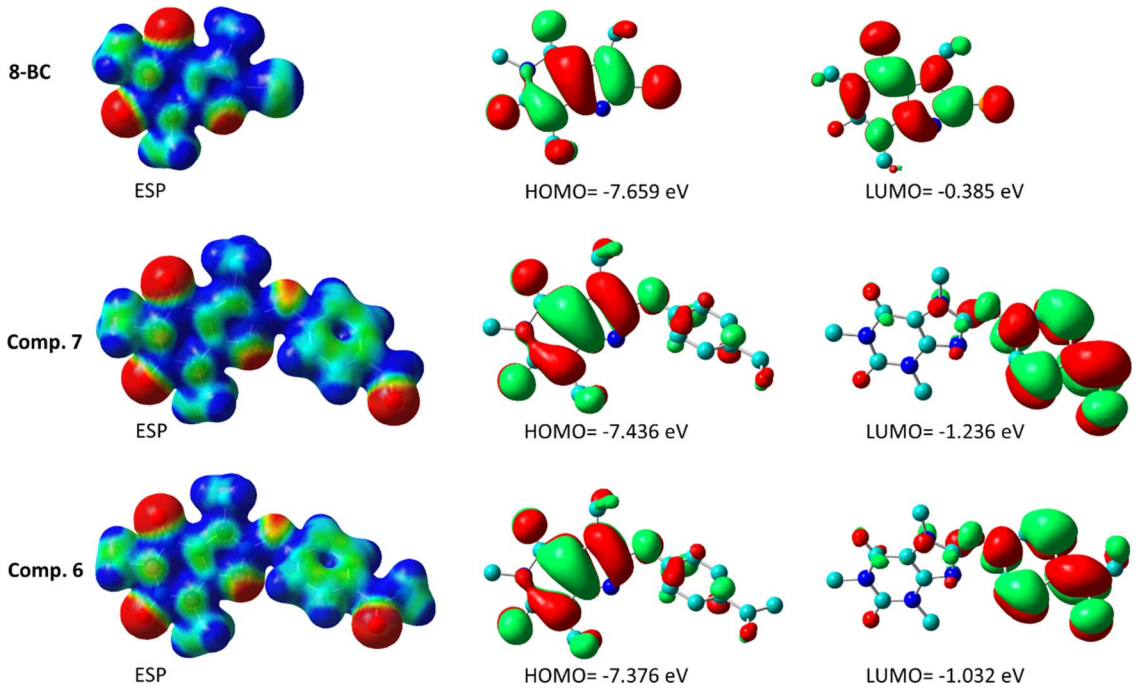

Fig. 14 ESP, HOMO, and LUMO of 8-BC, compounds **6** and **7**.

compounds **6**, **7**, and 8-BC are calculated by dividing the charge data into three parts: (i) the caffeinyl part before atom 15 (O or Br), (ii) atom 15, and (iii) the remaining atoms in both **6** and **7** after atom O15. The analysis reveals significant differences in the behavior of the caffeine moiety when Br is replaced with 4-carbonylphenoxy moiety. According to the NBO analysis results (Table 4), the presence of O15 in 4-carbonylphenoxy group influences the atoms on both sides of the molecule, leading to changes in the behavior of the caffeinyl core in both **6** and **7** compared to 8-BC.

Fig. 14 illustrates the electrostatic surface potential (ESP) of solute molecules, with all ESP maps sharing a common color range and isodensity value of 0.02. Additionally, Fig. 14 presents the HOMO and LUMO images of compounds **6**, **7**, and 8-BC in a solution. While the caffeinyl core influences both the HOMO and LUMO of 8-BC, compounds **6** and **7** exhibit the HOMO primarily on the caffeinyl part and the LUMO on the 4-carbonylphenoxy group, a key element for molecular reactivity. Substituting the bromine atom in 8-BC with 4-carbonylphenoxy moieties (bearing O15) to acquire **6** or **7** shifts the reactive site from caffeinyl core to a linked 4-carbonylphenoxy residue in **6** and **7**. The calculated HOMO–LUMO energy gaps for compounds **6**, **7**, and 8-BC are 6.344, 6.200, and 7.275 eV, respectively, indicating higher reactivity in **6** and **7** compared to 8-BC. This causes the side reaction of **6** and/or **7** with OH^- that led to formation of **8** as observed, experimentally.

3. Conclusion

In this paper, we conducted a comprehensive evaluation of the design, synthesis, characterization, anticancer properties, toxicity, and *in silico* analysis of novel 8-caffeinyl chalcone hybrid conjugates. These compounds were prepared by combining 8-BC with chalcones having diverse substituents. The synthesis process involved three stages: bromination of caffeine to produce 8-BC, synthesis of chalcones, and subsequent coupling of chalcones with 8-BC. The anticancer efficacy of these compounds was evaluated *in vitro* against two important cancer cell lines, breast cancer MCF-7 (ATCC HTB-22) and melanoma cancer A-375 (ATCC CRL-1619), with methotrexate (MTX) used as a reference drug. Among the compounds tested, **4k** showed the highest potency against A-375 ($IC_{50} = 92 \pm 3.2$), while **4d**, **4k**, **4e**, and **4a** exhibited significant inhibitory effects on MCF-7 cell growth, with their activities surpassing that of MTX. Toxicity assessments on the normal cell line HEK-293 (ATCC CRL-11268) revealed varying degrees of toxicity in the compounds, with exceptions noted for **4f**, **4g**, **5a**, and **5c–5e**, which demonstrated minimal toxicity. Molecular docking studies on **4k** and **5a** indicated strong binding affinities to B-RAF kinase and hDHFR enzymes. Furthermore, *in silico* pharmacokinetic and physiochemical profiling of the compounds showed that most adhered to Lipinski's rule of five (RO5). Additionally, density functional theory (DFT) calculations at the M06-2X-D3/6-31+G(d,p) level were employed to analyze atom charges, HOMO–LUMO energies, electrostatic potential (ESP), and other parameters of the intermediates, providing insights to support and elucidate the underlying mechanisms.

4. Experimental

4.1 Materials and cell lines

Cancer cell lines MCF-7 (ATCC HTB-22) derived from breast cancer, A-375 (ATCC CRL-1619) from melanoma, and the normal cell line HEK-293 (ATCC CRL-11268) were sourced from

the Pasteur Institute of Iran. Fetal bovine serum (FBS) was procured from Gibco (USA). Phosphate-buffered saline (PBS) tablets, tetrazolium salt, and MTT (3-(4,5-dimethyl-thiazol-2-yl)-2,5-diphenyltetrazolium bromide) were obtained from Sigma-Aldrich (USA). Dimethyl sulfoxide (DMSO), trypsin, penicillin/streptomycin, and Dulbecco's Modified Eagle's Media (DMEM) cell culture medium were supplied by Shellmax (China).

4.2 Evaluation of anticancer activity

The anticancer activity of the title compounds and MTX[43] was assessed using the MTT assay. All compounds were dissolved in a PBS solution containing 0.5% DMSO, and necessary dilutions were made using the same solvent.

The cell lines (MCF-7, A-375, and HEK-293) were cultured in culture flasks in DMEM complete medium (comprising 10% FBS and 1% penicillin–streptomycin) and then incubated at 37 °C in a CO_2 (5%) and air (95%) environment. Following separation using trypsin, the cell lines were seeded in 96-well plates and incubated for 48 hours. Subsequently, the culture media was removed, and each well was replenished with 75 μL of fresh complete medium. The compounds at concentrations of 15.62, 31.25, 62.5, 125, 250, and 500 μM were added to the wells. After another incubation period of 48 hours at 37 °C in a 95% air and 5% CO_2 atmosphere, the contents of the plates were discarded, and the wells were washed with 100 μL of PBS. Then, 100 μL of MTT solution (0.5 mg mL^{-1}) was added to each well and incubated for an additional 4 hours. Following this, 100 μL of DMSO was added to each well to dissolve the formazan crystals that were formed. In each plate, six wells served as the control group, containing a PBS solution with 0.5% DMSO (25 μL) and DMEM with the cells (75 μL). Finally, the absorbance (A) of each well was measured at 570 nm using an ELISA plate reader. The cell viability at each concentration was calculated using eqn (2).

$$\text{Cell viability}(\%) = \frac{\text{mean } A \text{ sample}}{\text{mean } A \text{ control}} \times 100 \quad (2)$$

4.2.1 Statistical analyses. Three repetitions were conducted for all tests, and the results were presented as the mean ± standard deviation. The final results of all samples were analyzed using the SPSS software with a one-way ANOVA at a 95% confidence level.

4.3 Molecular docking studies procedure

The molecular docking investigation was conducted utilizing Molegro Virtual Docker (MVD 6.0) software with its default settings.[34] For this study, the crystal structures of B-RAF V600E bound to vemurafenib (PDB code: 3OG7) and human DHFR bound to MTX and NADPH (PDB code: 1U72) were retrieved from the RCSB website. The enzyme structures were prepared by removing water molecules and ligands, adjusting hydrogen atoms, and ensuring accurate bond and atom assignments. Specifically, in the case of B-RAF V600E, chain B was excluded, and only chain A was used for docking. For hDHFR, the docking was performed with NADPH present. The docking simulations were run 50 times for each system. The active site of the enzymes was defined as residues within a 7 Å radius around the inhibitor ligand. The structures of vemurafenib, methotrexate, **4k**, and **5a** were optimized using the PM6 method in Gaussian09.[44,45] Initially, the docking was validated by re-docking vemurafenib and methotrexate into the active sites of B-RAF V600E and hDHFR, respectively. Subsequently, the optimized structures of ligands **4k** and **5a** were introduced into the analysis. The interactions were examined and assessed based on the docking outcomes using the Discovery Studio 2021 visualizer.

4.4 Chemistry general

All chemicals were bought from Merck and other chemical suppliers and directly used without additional purifications. The reactions were observed using TLC on SILG/UV 254 silica-gel plates. Purifications through short column chromatography were carried out using silica gel 60 (mesh size 0.063–0.200 mm, 70–230 mesh; ASTM). Melting points were taken using the Electrothermal IA 9000 in open capillary tubes without correction. Elemental analyses, GC/MS, and IR spectra were obtained using the PerkinElmer 240-B micro-analyzer, Shimadzu GC/MS-QP 1000-EX apparatus (m/z; rel.%), and the Shimadzu FT-IR-8300 spectrophotometer, respectively. ^{1}H- and ^{13}C-NMR spectra were recorded on the Brüker Avance-DPX-300 spectrometer operating at 300/75 MHz, respectively. Chemical shifts are referenced in δ relative to tetramethylsilane (TMS) as an internal standard, and coupling constants J are given in Hz. Abbreviations used for ^{1}H-NMR signals include s = singlet, d = doublet, t = triplet, q = quartet, m = multiplet, br = broad, *etc.*

4.4.1 Synthesis of 8-bromo-1,3,7-trimethyl-1*H*-purine-2,6(3*H*,7*H*)-dione (8-BC). Caffeine (19.4 g, 0.1 mol) and NBS (35.2 g, 0.2 mol) were added to 300 mL of freshly distilled DCM in a 500 mL round-bottom flask. After the solids dissolved, 100 mL of water was added, and the mixture was vigorously shaken for 5–7 days at room temperature (checked using TLC). The solution was then transferred to a separator funnel, where a solution of cold NaOH (100 mL, 2 M) was added and shaken to remove color from the mixture. The organic layer was separated, washed with water twice (200 mL each), dried over Na_2SO (30 g), filtered, and evaporated to yield pure 8-BC (26 g, approximately 100% yield).

4.4.2 Synthesis of chalcone's series 9. In a 100 mL double-necked round bottom flask fitted with a condenser, a mixture of 4-hydroxyacetophenone (1.36 g, 10 mmol) and the desired aldehyde (11 mmol) in 30 mL of ethanol (90%) was placed. The mixture was stirred and gently refluxed, while a solution of 20 mmol NaOH in 5 mL distilled water was slowly added to the reaction medium. The progress of the reaction was monitored using TLC. Once TLC analysis indicated completion of the reaction (approximately 6–8 hours), the reaction was terminated and the solution was allowed to cool to room temperature. The reaction mixture was neutralized with 5 M HCl, and the resulting precipitate was filtered, washed with 3 portions of distilled water (50 mL each), and finally recrystallized in hot ethanol or methanol.

4.4.3 Synthesis of chalcone's series 10. In a 100 mL double-necked round bottom flask equipped with a condenser, a mixture of 4-hydroxybenzaldehyde (1.22 g, 10 mmol) and the desired aromatic methyl ketone (11 mmol) in 30 mL of ethanol (90%) was added. The mixture was stirred and gently refluxed, while a solution of 5 mL 36% HCl and 5 mL 98% H_2SO_4 was slowly introduced to the reaction mixture. The progress of the reaction was monitored using TLC. Once TLC analysis indicated the reaction was complete (after 12–24 hours), the reaction was halted, and the solution was cooled to room temperature. The reaction mixture was neutralized with a saturated solution of Na_2CO_3, and the resulting precipitates were filtered, washed with three portions of distilled water (50 mL each), and finally recrystallized in hot ethanol or methanol.

4.4.4 General procedure A: synthesis of 8-caffeinyl chalcone hybrid conjugates 4a–4k. A 100 mL round bottom flask with two necks and a condenser attached was prepared. A mixture of 8-BC (2.73 g, 10 mmol), the desired chalcone **9** (10 mmol), and K_2CO_3 (1.38, 10 mmol) in anhydrous DMF (20 mL) was added to the flask. The contents were stirred and heated to 60 °C. The reaction progress was monitored using TLC. Once the TLC indicated that the reaction was complete after an appropriate duration (refer to Scheme 3), the reaction was halted, and the solution was allowed to cool to room temperature. The reaction mixture was then diluted with distilled water, and the resulting precipitates were filtered, washed with distilled water (3 × 100 mL). The solid obtained was pure enough without requiring further purification and it was dried under vacuum at 50 °C which subsequently sealed and kept in refrigerator.

4.4.5 Data of the synthesized compounds 4a–4k

*4.4.5.1 (E)-1,3,7-Trimethyl-8-(4-(3-p-tolylacryloyl)phenoxy)-1H-purine-2,6(3H,7H)-dione (**4a**).* Compound **4a** was obtained according to the general procedure A from a mixture of 8-BC (2.73 g, 10 mmol), (*E*)-1-(4-hydroxyphenyl)-3-*p*-tolylprop-2-en-1-one (2.38 g, 10 mmol), and K_2CO_3 (1.38, 10 mmol) in anhydrous DMF (20 mL) after 12 h as pale orange solid (3.52 g, 82%); m.p.: 166–168 °C, ^{1}H NMR ($CDCl_3$, 400 MHz): δ_{ppm} = 8.13 (d, J = 8.8 Hz, 2H, aryl), 7.85 (d, J = 15.6 Hz, 1H, C(O)–CH), 7.57–7.46 (complex, 5H, aryl, C(O)–CH=CH), 7.25 (d, J = 8.0 Hz, 2H, aryl), 3.91 (s, 3H, N(7)-CH_3), 3.48 (s, 3H, N(3)-CH_3), 3.42 (s, 3H, N(1)-CH_3), 2.41 (s, 3H, PhCH_3). ^{13}C NMR ($CDCl_3$, 100 MHz): δ_{ppm} = 188.61, 156.87, 154.81, 152.03, 151.31, 145.64, 144.58, 134.29, 133.11, 130.79, 129.85, 129.03, 128.21, 121.41, 119.82, 104.03, 30.69, 29.53, 27.58, 21.81. IR (KBr): 3050, 2986, 1705, 1697, 1652, 1553, 1484, 1275, 1056 cm^{-1}. MS (EI): m/z (%) = 430 (27.5) [M^+]. Anal. calc. for $C_{24}H_{22}N_4O_4$: C, 66.97; H, 5.15; N, 13.02; found: C, 66.85; H, 5.29; N, 13.14.

*4.4.5.2 (E)-8-(4-(3-(2,4-Dichlorophenyl)acryloyl)phenoxy)-1,3,7-trimethyl-1H-purine-2,6(3H,7H)-dione (**4b**).* Compound **4b** was obtained according to the general procedure A from a mixture of 8-BC (2.73 g, 10 mmol), (*E*)-3-(2,4-dichlorophenyl)-1-(4-hydroxyphenyl)prop-2-en-1-one (2.93 g, 10 mmol), and K_2CO_3 (1.38, 10 mmol) in anhydrous DMF (20 mL) after 14 h as creamy solid (4.27 g, 88%); m.p.: 180–182 °C, ^{1}H NMR ($CDCl_3$, 400 MHz): δ_{ppm} = 8.16–8.11 (m, 3H, aryl), 7.71 (d, J = 15.6 Hz, 1H, C(O)–CH), 7.50–7.47 (complex, 4H, aryl, C(O)–CH=CH), 7.33 (d, J = 10.4 Hz, 1H, aryl), 3.92 (s, 3H, N(7)-CH_3), 3.49 (s, 3H, N(3)-CH_3), 3.42 (s, 3H, N(1)-CH_3). ^{13}C NMR ($CDCl_3$, 100 MHz): δ_{ppm} = 188.65, 156.62, 154.58, 152.46, 151.34, 145.72, 141.17, 135.97, 135.01, 133.25, 131.49, 130.38, 129.46, 127.76, 126.91, 124.38, 119.49, 104.07, 30.51, 29.37, 27.82. IR (KBr): 3028, 2972, 1706, 1695, 1650, 1561, 1480, 1268, 1050, 870 cm^{-1}. MS (EI): m/z (%) = 484 (34.8) [M^+]. Anal. calc. for $C_{23}H_{18}Cl_2N_4O_4$: C, 56.92; H, 3.74; N, 11.54; found: C, 57.11; H, 3.91; N, 11.70.

*4.4.5.3 (E)-8-(4-(3-(2-Methoxyphenyl)acryloyl)phenoxy)-1,3,7-trimethyl-1H-purine-2,6(3H,7H)-dione (**4c**).* Compound **4c** was obtained according to the general procedure A from a mixture of 8-BC (2.73 g, 10 mmol), (*E*)-1-(4-hydroxyphenyl)-3-(2-methoxyphenyl)prop-2-en-1-one (2.54 g, 10 mmol), and K_2CO_3 (1.38, 10 mmol) in anhydrous DMF (20 mL) after 12 h as yellow solid (4.15 g, 93%); m.p.: 166–168 °C, ^{1}H NMR ($CDCl_3$, 400 MHz): δ_{ppm} = 8.17 (br s, 1H, C(O)–CH), 8.13 (d, J = 8.4 Hz, 2H, aryl), 7.66–7.62 (complex, 2H, C(O)–CH=CH, aryl), 7.47 (d, J = 8.8 Hz, 2H, aryl), 7.43 (t, J = 7.6 Hz, 1H, aryl), 7.04–6.96 (m, 2H, aryl), 3.94 (s, 3H, N(7)-CH_3), 3.91 (s, 3H, N(3)-CH_3), 3.49 (s, 3H, N(1)-CH_3), 3.43 (s, 3H, OCH_3). ^{13}C NMR ($CDCl_3$, 100 MHz): δ_{ppm} = 188.57, 156.51, 155.07, 152.43, 151.49, 150.75, 149.35, 145.85, 144.98, 135.83, 130.58, 127.70, 123.34, 120.02, 119.33, 114.32, 112.53, 103.96, 55.76, 30.69, 29.90, 27.58. IR (KBr): 3075, 2959, 1703, 1692, 1657, 1552, 1465, 1268, 1059 cm^{-1}. MS (EI): m/z (%) = 446 (29.2) [M^+]. Anal. calc. for $C_{24}H_{22}N_4O_5$: C, 64.57; H, 4.97; N, 12.55; found: C, 64.40; H, 5.06; N, 12.42.

*4.4.5.4 (E)-8-(4-Cinnamoylphenoxy)-1,3,7-trimethyl-1H-purine-2,6(3H,7H) dione (**4d**).* Compound **4d** was obtained according to the general procedure A from a mixture of 8-BC (2.73 g, 10 mmol), (*E*)-1-(4-hydroxyphenyl)-3-phenylprop-2-en-1-one (2.24 g, 10 mmol), and K_2CO_3 (1.38, 10 mmol) in anhydrous DMF (20 mL) after 12 h as pale creamy solid (3.45 g, 83%); m.p.: 165–167 °C, ^{1}H NMR ($CDCl_3$, 400 MHz): δ_{ppm} = 8.14 (d, J = 8.8 Hz, 2H, aryl), 7.87 (d, J = 15.6 Hz, 1H, C(O)–CH), 7.68–7.66 (m, 2H, aryl), 7.57 (d, J = 15.6 Hz, 1H, C(O)–CH=CH), 7.49–7.44 (m, 5H, aryl), 3.92 (s, 3H, N(7)-CH_3), 3.49 (s, 3H, N(3)-CH_3), 3.42 (s, 3H, N(1)-CH_3). ^{13}C NMR ($CDCl_3$, 100 MHz): δ_{ppm} = 188.83, 156.58, 154.95, 152.43, 151.59, 145.66, 145.25, 135.48, 134.72, 130.75, 130.56, 129.02, 128.50, 121.51, 119.25, 103.97, 30.58, 29.91, 27.88. IR (KBr): 3068, 2971, 1706, 1697, 1662, 1541, 1460, 1260, 1051 cm^{-1}. MS (EI): m/z (%) = 416 (23.9) [M^+]. Anal. calc. for $C_{23}H_{20}N_4O_4$: C, 66.34; H, 4.84; N, 13.45; found: C, 66.53; H, 5.01; N, 13.63.

*4.4.5.5 (E)-8-(4-(3-(4-Chlorophenyl)acryloyl)phenoxy)-1,3,7-trimethyl-1H-purine-2,6(3H,7H)-dione (**4e**).* Compound **4e** was obtained according to the general procedure A from a mixture of 8-BC (2.73 g, 10 mmol), (*E*)-3-(4-chlorophenyl)-1-(4-hydroxyphenyl)prop-2-en-1-one (2.58 g, 10 mmol), and K_2CO_3 (1.38, 10 mmol) in anhydrous DMF (20 mL) after 12 h as pale orange solid (4.23 g, 94%); m.p.: 110–112 °C, ^{1}H NMR ($CDCl_3$, 400 MHz): δ_{ppm} = 8.14 (d, J = 8.8 Hz, 2H, aryl), 7.82 (d, J = 15.6 Hz, 1H, C(O)–CH), 7.61 (d, J = 8.4 Hz, 2H, aryl), 7.54–7.41 (complex, 5H, C(O)–CH=CH, aryl), 3.92 (s, 3H, N(7)-CH_3), 3.49 (s, 3H, N(3)-CH_3), 3.43 (s, 3H, N(1)-CH_3). ^{13}C NMR ($CDCl_3$, 100 MHz): δ_{ppm} = 188.53, 156.67, 154.96, 152.39, 151.59, 145.65, 143.73, 136.66, 135.28, 133.20, 130.57, 129.65, 129.32, 121.87,

119.30, 104.01, 30.59, 29.92, 27.90. IR (KBr): 3100, 2980, 1707, 1694, 1658, 1550, 1459, 1280, 1057, 840 cm^{-1}. MS (EI): *m*/*z* (%) = 450 (30.1) [M^+]. Anal. calc. for $C_{23}H_{19}ClN_4O_4$: C, 61.27; H, 4.25; N, 12.43; found: C, 61.09; H, 4.06; N, 12.27.

*4.4.5.6 (E)-1,3,7-Trimethyl-8-(4-(3-(3-nitrophenyl)acryloyl) phenoxy)-1H-purine-2,6(3H,7H)-dione (**4f**).* Compound **4f** was obtained according to the general procedure A from a mixture of 8-BC (2.73 g, 10 mmol), (*E*)-1-(4-hydroxyphenyl)-3-(3-nitrophenyl)prop-2-en-1-one (2.69 g, 10 mmol), and K_2CO_3 (1.38, 10 mmol) in anhydrous DMF (20 mL) after 18 h as yellow solid (3.27 g, 71%); m.p.: 277–279 °C, ^{1}H NMR ($CDCl_3$, 400 MHz): δ_{ppm} = 8.31 (br s, 1H, C(O)–CH), 8.06–7.63 (complex, 5H, aryl, C(O)–CH=CH), 7.46–7.29 (complex, 3H, aryl), 7.04 (s, 1H, aryl), 3.69 (s, 3H, N(7)-CH_3), 3.25 (s, 3H, N(3)-CH_3), 3.19 (s, 3H, N(1)-CH_3). ^{13}C NMR ($CDCl_3$, 100 MHz): δ_{ppm} = 187.99, 156.96, 154.96, 151.59, 148.65, 145.63, 141.93, 140.84, 137.37, 134.78, 130.71, 129.01, 125.15, 124.27, 123.55, 119.45, 115.70, 104.05, 30.61, 29.92, 27.92. IR (KBr): 3050, 2970, 1705, 1698, 1663, 1565, 1548, 1449, 1351, 1260, 1053 cm^{-1}. MS (EI): *m*/*z* (%) = 461 (21.4) [M^+]. Anal. calc. for $C_{23}H_{19}N_5O_6$: C, 59.87; H, 4.15; N, 15.18; found: C, 60.02; H, 4.33; N, 15.31.

*4.4.5.7 (E)-8-(4-(3-(2,4-Dimethoxyphenyl)acryloyl)phenoxy)-1,3,7-trimethyl-1H-purine-2,6(3H,7H)-dione (**4g**).* Compound **4g** was obtained according to the general procedure A from a mixture of 8-BC (2.73 g, 10 mmol), (*E*)-3-(2,4-dimethoxyphenyl)-1-(4-hydroxyphenyl)prop-2-en-1-one (2.84 g, 10 mmol), and K_2CO_3 (1.38, 10 mmol) in anhydrous DMF (20 mL) after 12 h as orange solid (4.19 g, 88%); m.p.: 216–218 °C, ^{1}H NMR ($CDCl_3$, 400 MHz): δ_{ppm} = 8.13 (d, *J* = 8.8 Hz, 2H, aryl), 7.82 (d, *J* = 15.6 Hz, 1H, C(O)–CH), 7.48 (d, *J* = 15.2 Hz, 2H, aryl), 7.42 (d, *J* = 15.2 Hz, 1H, C(O)–CH=CH), 7.27 (d, *J* = 8.4 Hz, 1H, aryl), 7.17 (br s, 1H, aryl), 6.93 (d, *J* = 8.4 Hz, 1H, aryl), 3.96 (s, 3H, OCH_3), 3.95 (s, 3H, OCH_3), 3.91 (s, 3H, N(7)-CH_3), 3.48 (s, 3H, N(3)-CH_3), 3.42 (s, 3H, N(1)-CH_3). ^{13}C NMR ($CDCl_3$, 100 MHz): δ_{ppm} = 188.90, 156.43, 154.95, 152.47, 151.61, 151.58, 149.27, 145.66, 145.46, 135.75, 130.47, 127.67, 123.32, 119.42, 119.20, 111.12, 110.09, 103.96, 56.04, 55.99, 30.58, 29.91, 27.88. IR (KBr): 3035, 2968, 1704, 1694, 1660, 1550, 1462, 1270, 1049 cm^{-1}. MS (EI): *m*/*z* (%) = 476 (28.3) [M^+]. Anal. calc. for $C_{25}H_{24}N_4O_6$: C, 63.02; H, 5.08; N, 11.76; found: C, 62.86; H, 5.21; N, 11.90.

*4.4.5.8 (E)-8-(4-(3-(4-Methoxyphenyl)acryloyl)phenoxy)-1,3,7-trimethyl-1H-purine-2,6(3H,7H)-dione (**4h**).* Compound **4h** was obtained according to the general procedure A from a mixture of 8-BC (2.73 g, 10 mmol), (*E*)-1-(4-hydroxyphenyl)-3-(4-methoxyphenyl)prop-2-en-1-one (2.54 g, 10 mmol), and K_2CO_3 (1.38, 10 mmol) in anhydrous DMF (20 mL) after 14 h as creamy solid (4.10 g, 92%); m.p.: 153–155 °C, ^{1}H NMR ($CDCl_3$, 400 MHz): δ_{ppm} = 8.13 (d, *J* = 8.8 Hz, 2H, aryl), 7.85 (d, *J* = 15.6 Hz, 1H, C(O)–CH), 7.64 (d, *J* = 8.8 Hz, 2H, aryl), 7.48–7.41 (complex, 3H, C(O)–CH=CH, aryl), 6.97 (d, *J* = 8.8 Hz, 2H, aryl), 3.91 (s, 3H, OCH_3), 3.88 (s, 3H, N(7)-CH_3), 3.49 (s, 3H, N(3)-CH_3), 3.42 (s, 3H, N(1)-CH_3). ^{13}C NMR ($CDCl_3$, 100 MHz): δ_{ppm} = 188.87, 161.84, 156.41, 154.96, 152.50, 151.60, 145.68, 145.12, 135.79, 130.45, 130.33, 127.44, 119.20, 119.15, 114.48, 103.97, 55.46, 30.58, 29.92, 27.89. IR (KBr): 3085, 2947, 1706, 1699, 1656, 1550, 1472, 1283, 1060 cm^{-1}. MS (EI): *m*/*z* (%) = 446 (24.9) [M^+]. Anal. calc. for $C_{24}H_{22}N_4O_5$: C, 64.57; H, 4.97; N, 12.55; found: C, 64.76; H, 5.12; N, 12.69.

*4.4.5.9 (E)-8-(4-(3-(2-Chlorophenyl)acryloyl)phenoxy)-1,3,7-trimethyl-1H-purine-2,6(3H,7H)-dione (**4i**).* Compound **4i** was obtained according to the general procedure A from a mixture of 8-BC (2.73 g, 10 mmol), (*E*)-3-(2-chlorophenyl)-1-(4-hydroxyphenyl)prop-2-en-1-one (2.58 g, 10 mmol), and K_2CO_3 (1.38, 10 mmol) in anhydrous DMF (20 mL) after 13 h as yellow solid (4.05 g, 90%); m.p.: 173–175 °C, ^{1}H NMR ($CDCl_3$, 400 MHz): δ_{ppm} = 8.22 (d, *J* = 15.6 Hz, 1H, C(O)–CH), 8.12 (d, *J* = 8.8 Hz, 2H, aryl), 7.76–7.74 (m, 1H, C(O)–CH=CH) 7.51–7.44 (m, 4H, aryl), 7.37–7.30 (m, 2H, aryl), 3.90 (s, 3H, N(7)-CH_3), 3.47 (s, 3H, N(3)-CH_3), 3.41 (s, 3H, N(1)-CH_3). ^{13}C NMR ($CDCl_3$, 100 MHz): δ_{ppm} = 188.80, 156.67, 154.93, 152.40, 151.57, 145.64, 141.00, 135.54, 135.15, 133.04, 131.38, 130.69, 130.36, 127.79, 127.13, 124.26, 119.30, 103.97, 30.58, 29.92, 27.89. IR (KBr): 3037, 2962, 1705, 1696, 1658, 1557, 1479, 1270, 1054, 857 cm^{-1}. MS (EI): *m*/*z* (%) = 450 (26.7) [M^+]. Anal. calc. for $C_{23}H_{19}ClN_4O_4$: C, 61.27; H, 4.25; N, 12.43; found: C, 61.41; H, 4.09; N, 12.26.

*4.4.5.10 (E)-8-(4-(3-(2,6-Dichlorophenyl)acryloyl)phenoxy)-1,3,7-trimethyl-1H-purine-2,6(3H,7H)-dione (**4j**).* Compound **4j** was obtained according to the general procedure A from a mixture of 8-BC (2.73 g, 10 mmol), (*E*)-3-(2,6-dichlorophenyl)-1-(4-hydroxyphenyl)prop-2-en-1-one (2.93 g, 10 mmol), and K_2CO_3 (1.38, 10 mmol) in anhydrous DMF (20 mL) after 16 h as green solid (4.27 g, 88%); m.p.: 216–218 °C, ^{1}H NMR ($CDCl_3$, 400 MHz): δ_{ppm} = 8.13 (d, *J* = 8.8 Hz, 2H, aryl), 7.91 (d, *J* = 16.0 Hz, 1H, C(O)–CH), 7.70 (d, *J* = 16.0 Hz, 1H, C(O)–CH=CH), 7.49 (d, *J* = 8.4 Hz, 2H, aryl), 7.41 (d, *J* = 8.0 Hz, 2H, aryl), 7.25 (t, *J* = 8.0 Hz, 1H, aryl), 3.91 (s, 3H, N(7)-CH_3), 3.48 (s, 3H, N(3)-CH_3), 3.41 (s, 3H, N(1)-CH_3). ^{13}C NMR ($CDCl_3$, 100 MHz): δ_{ppm} = 188.56, 156.81, 154.94, 152.36, 151.58, 145.64, 138.19, 135.19, 134.90, 132.43, 130.82, 130.02, 129.99, 128.92, 119.34, 103.97, 30.59, 29.93, 27.89. IR (KBr): 3070, 2978, 1703, 1695, 1648, 1559, 1467, 1281, 1053, 859 cm^{-1}. MS (EI): *m*/*z* (%) = 484 (19.4) [M^+]. Anal. calc. for $C_{23}H_{18}Cl_2N_4O_4$: C, 56.92; H, 3.74; N, 11.54; found: C, 57.10; H, 3.90; N, 11.67.

*4.4.5.11 (E)-Methyl 4-(3-oxo-3-(4-(1,3,7-trimethyl-2,6-dioxo-2,3,6,7-tetrahydro-1H-purin-8-yloxy)phenyl)prop-1-enyl)benzoate (**4k**).* Compound **4k** was obtained according to the general procedure A from a mixture of 8-BC (2.73 g, 10 mmol), (*E*)-methyl 4-(3-(4-hydroxyphenyl)-3-oxoprop-1-enyl)benzoate (2.82 g, 10 mmol), and K_2CO_3 (1.38, 10 mmol) in anhydrous DMF (20 mL) after 15 h as pale yellow solid (4.22 g, 89%); m.p.: 235–237 °C, ^{1}H NMR (DMSO-d_6, 400 MHz): δ_{ppm} = 8.30 (d, *J* = 8.4 Hz, 2H, aryl), 8.03–7.95 (complex, 3H, C(O)–CH, aryl), 7.88 (d, *J* = 3.2 Hz, 2H, aryl), 7.79 (d, *J* = 15.6 Hz, 1H, C(O)–CH=CH), 7.58 (d, *J* = 8.8 Hz, 2H, aryl), 3.80 (s, 3H, N(7)-CH_3), 3.30 (s, 3H, N(3)-CH_3), 3.23 (s, 3H, N(1)-CH_3), 2.09 (s, 3H, OCH_3). ^{13}C NMR (DMSO-d_6, 100 MHz): δ_{ppm} = 188.82, 170.34, 161.86, 156.85, 154.89, 152.61, 151.12, 145.95, 144.90, 135.81, 130.74, 129.60, 127.37, 119.94, 118.95, 114.71, 103.93, 54.02, 30.60, 29.90, 27.82. IR (KBr): 3067, 2958, 1730, 1705, 1697, 1659, 1550, 1477, 1279, 1180, 1061 cm^{-1}. MS (EI): *m*/*z* (%) = 474 (21.7) [M^+]. Anal. calc. for $C_{25}H_{22}N_4O_6$: C, 63.29; H, 4.67; N, 11.81; found: C, 63.41; H, 4.82; N, 11.65.

4.4.6 General procedure B: synthesis of 8-caffeinyl chalcone hybrid conjugates 5a–5f. A 100 mL round bottom flask with two necks and a condenser attached was prepared. A mixture of 8-BC (2.73 g, 10 mmol), the desired chalcone **10** (10 mmol), and K_2CO_3 (1.38, 10 mmol) in anhydrous DMF (20 mL) was added to the flask. The contents were stirred and heated to 60 °C. The reaction progress was monitored using TLC. Once the TLC indicated that the reaction was complete after an appropriate duration (refer to Scheme 3), the reaction was halted, and the solution was allowed to cool to room temperature. The reaction mixture was then diluted with distilled water, and the resulting precipitates were filtered, washed with distilled water (3 × 100 mL). The solid obtained was pure enough without requiring further purification and it was dried under vacuum at 50 °C which subsequently sealed and kept in refrigerator.

4.4.7 Data of the synthesized compounds 5a–5f

*4.4.7.1 (E)-8-(4-(3-(4-Methoxyphenyl)-3-oxoprop-1-enyl)phenoxy)-1,3,7-trimethyl-1H-purine-2,6(3H,7H)-dione (**5a**).* Compound **5a** was obtained according to the general procedure B from a mixture of 8-BC (2.73 g, 10 mmol), (*E*)-3-(4-hydroxyphenyl)-1-(4-methoxyphenyl)prop-2-en-1-one (2.54 g, 10 mmol), and K_2CO_3 (1.38, 10 mmol) in anhydrous DMF (20 mL) after 16 h as brown solid (4.15 g, 93%); m.p.: 139–141 °C, ^{1}H NMR ($CDCl_3$, 400 MHz): δ_{ppm} = 8.07–8.02 (complex, 3H, C(O)–CH=CH, aryl), 7.83–7.70 (complex, 3H, C(O)–CH, aryl), 7.56–7.52 (m, 2H, aryl), 7.43–7.38 (m, 2H, aryl), 3.91 (s, 3H, OCH_3), 3.89 (s, 3H, N(7)-CH_3), 3.48 (s, 3H, N(3)-CH_3), 3.43 (s, 3H, N(1)-CH_3). ^{13}C NMR ($CDCl_3$, 100 MHz): δ_{ppm} = 188.57, 163.61, 159.01, 154.58, 151.64, 144.33, 142.57, 132.63, 130.87, 129.86, 127.16, 122.07, 119.84, 116.07, 113.79, 104.02, 55.50, 30.53, 29.95, 27.92. IR (KBr): 3045, 2981, 1704, 1695, 1657, 1548, 1460, 1273, 1039 cm^{-1}. MS (EI): *m*/*z* (%) = 446 (20.2) [M$^+$]. Anal. calc. for $C_{24}H_{22}N_4O_5$: C, 64.57; H, 4.97; N, 12.55; found: C, 64.38; H, 4.81; N, 12.43.

*4.4.7.2 (E)-1,3,7-Trimethyl-8-(4-(3-(4-nitrophenyl)-3-oxoprop-1-enyl)phenoxy)-1H-purine-2,6(3H,7H)-dione (**5b**).* Compound **5b** was obtained according to the general procedure B from a mixture of 8-BC (2.73 g, 10 mmol), (*E*)-3-(4-hydroxyphenyl)-1-(4-nitrophenyl)prop-2-en-1-one (2.69 g, 10 mmol), and K_2CO_3 (1.38, 10 mmol) in anhydrous DMF (20 mL) after 18 h as pale orange solid (3.69 g, 80%); m.p.: 250–252 °C, ^{1}H NMR ($CDCl_3$, 400 MHz): δ_{ppm} = 8.40 (d, *J* = 8.8 Hz, 2H, aryl), 8.18 (d, *J* = 8.4 Hz, 2H, aryl), 7.90 (d, *J* = 16.0 Hz, 1H, C(O)–CH=CH), 7.77 (d, *J* = 8.8 Hz, 2H, aryl), 7.51–7.43 (complex, 3H, C(O)–CH, aryl), 3.92 (s, 3H, N(7)-CH_3), 3.50 (s, 3H, N(3)-CH_3), 3.43 (s, 3H, N(1)-CH_3). ^{13}C NMR ($CDCl_3$, 100 MHz): δ_{ppm} = 188.74, 155.25, 152.59, 151.61, 150.13, 145.27, 143.20, 142.88, 131.78, 130.86, 130.27, 129.42, 123.93, 121.40, 119.97, 106.21, 30.56, 29.92, 27.90. IR (KBr): 3036, 2975, 1706, 1698, 1656, 1559, 1530, 1450, 1341, 1267, 1052 cm^{-1}. MS (EI): *m*/*z* (%) = 461 (25.8) [M$^+$]. Anal. calc. for $C_{23}H_{19}N_5O_6$: C, 59.87; H, 4.15; N, 15.18; found: C, 59.69; H, 4.03; N, 15.01.

*4.4.7.3 (E)-1,3,7-Trimethyl-8-(4-(3-(3-nitrophenyl)-3-oxoprop-1-enyl)phenoxy)-1H-purine-2,6(3H,7H)-dione (**5c**).* Compound **5c** was obtained according to the general procedure B from a mixture of 8-BC (2.73 g, 10 mmol), (*E*)-3-(4-hydroxyphenyl)-1-(3-nitrophenyl)prop-2-en-1-one (2.69 g, 10 mmol), and K_2CO_3 (1.38, 10 mmol) in anhydrous DMF (20 mL) after 16 h as yellow solid (3.92 g, 85%); m.p.: 248–250 °C, ^{1}H NMR ($CDCl_3$, 400 MHz): δ_{ppm} = 8.87 (br s, 1H, C(O)–CH=CH), 8.49–8.39 (m, 2H, aryl), 7.94–7.78 (complex, 4H, C(O)–CH, aryl), 7.56–7.46 (m, 3H, aryl), 3.92 (s, 3H, N(7)-CH_3), 3.50 (s, 3H, N(3)-CH_3), 3.43 (s, 3H, N(1)-CH_3). ^{13}C NMR ($CDCl_3$, 100 MHz): δ_{ppm} = 188.93, 155.67, 154.86, 152.75, 151.65, 145.82, 143.75, 142.64, 135.68, 132.64, 130.17, 129.46, 128.26, 127.65, 126.97, 122.57, 119.98, 104.04, 30.69, 29.81, 27.89. IR (KBr): 3050, 2968, 1705, 1693, 1658, 1564, 1545, 1479, 1350, 1282, 1051 cm^{-1}. MS (EI): *m*/*z* (%) = 461 (30.6) [M$^+$]. Anal. calc. for $C_{23}H_{19}N_5O_6$: C, 59.87; H, 4.15; N, 15.18; found: C, 60.04; H, 4.29; N, 15.37.

*4.4.7.4 (E)-1,3,7-Trimethyl-8-(4-(3-oxo-3-p-tolylprop-1-enyl)phenoxy)-1H-purine-2,6(3H,7H)-dione (**5d**).* Compound **5d** was obtained according to the general procedure B from a mixture of 8-BC (2.73 g, 10 mmol), (*E*)-3-(4-hydroxyphenyl)-1-*p*-tolylprop-2-en-1-one (2.38 g, 10 mmol), and K_2CO_3 (1.38, 10 mmol) in anhydrous DMF (20 mL) after 13 h as creamy solid (3.44 g, 80%); m.p.: 201–203 °C, ^{1}H NMR ($CDCl_3$, 400 MHz): δ_{ppm} = 7.96 (d, *J* = 8.0 Hz, 2H, aryl), 7.83 (d, *J* = 16.0 Hz, 1H, C(O)–CH=CH), 7.73 (d, *J* = 8.8 Hz, 2H, aryl), 7.55 (d, *J* = 15.6 Hz, 1H, C(O)–CH), 7.41 (d, *J* = 8.8 Hz, 2H, aryl), 7.33 (d, *J* = 8.0 Hz, 2H, aryl), 3.90 (s, 3H, N(7)-CH_3), 3.48 (s, 3H, N(3)-CH_3), 3.42 (s, 3H, N(1)-CH_3), 2.45 (s, 3H, $PhCH_3$). ^{13}C NMR ($CDCl_3$, 100 MHz): δ_{ppm} = 189.65, 154.94, 154.65, 152.79, 151.60, 145.72, 143.86, 142.87, 135.47, 132.53, 129.89, 129.40, 128.65, 122.24, 119.82, 103.87, 30.52, 29.91, 27.87, 21.72. IR (KBr): 3072, 2980, 1707, 1696, 1645, 1566, 1457, 1270, 1063 cm^{-1}. MS (EI): *m*/*z* (%) = 430 (18.2) [M$^+$]. Anal. calc. for $C_{24}H_{22}N_4O_4$: C, 66.97; H, 5.15; N, 13.02; found: C, 66.85; H, 5.34; N, 13.16.

*4.4.7.5 (E)-1,3,7-Trimethyl-8-(4-(3-(naphthalen-2-yl)-3-oxoprop-1-enyl)phenoxy)-1H-purine-2,6(3H,7H)-dione (**5e**).* Compound **5e** was obtained according to the general procedure B from a mixture of 8-BC (2.73 g, 10 mmol), (*E*)-3-(4-hydroxyphenyl)-1-(naphthalen-2-yl)prop-2-en-1-one (2.74 g, 10 mmol), and K_2CO_3 (1.38, 10 mmol) in anhydrous DMF (20 mL) after 13 h as brown solid (4.05 g, 87%); m.p.: 175–177 °C, ^{1}H NMR ($CDCl_3$, 400 MHz): δ_{ppm} = 8.13 (d, *J* = 15.6 Hz, 1H, C(O)–CH=CH), 8.02–7.87 (complex, 5H, C(O)–CH, aryl), 7.78 (d, *J* = 8.4 Hz, 2H, aryl), 7.72–7.61 (m, 3H, aryl), 7.44 (d, *J* = 8.8 Hz, 2H, aryl), 3.91 (s, 3H, N(7)-CH_3), 3.49 (s, 3H, N(3)-CH_3), 3.42 (s, 3H, N(1)-CH_3). ^{13}C NMR ($CDCl_3$, 100 MHz): δ_{ppm} = 190.03, 154.92, 154.74, 152.79, 143.30, 135.54, 135.38, 132.53, 132.49, 130.02, 129.52, 128.68, 128.54, 127.87, 127.80, 126.90, 124.41, 122.22, 119.88, 103.87, 30.54, 29.94, 27.90. IR (KBr): 3046, 2968, 1705, 1697, 1660, 1559, 1474, 1283, 1050 cm^{-1}. MS (EI): *m*/*z* (%) = 466 (35.3) [M$^+$]. Anal. calc. for $C_{27}H_{22}N_4O_4$: C, 69.52; H, 4.75; N, 12.01; found: C, 69.64; H, 4.91; N, 12.16.

*4.4.7.6 (E)-8-(4-(3-(4-Chlorophenyl)-3-oxoprop-1-enyl)phenoxy)-1,3,7-trimethyl-1H-purine-2,6(3H,7H)-dione (**5f**).* Compound **5f** was obtained according to the general procedure B from a mixture of 8-BC (2.73 g, 10 mmol), (*E*)-1-(4-chlorophenyl)-3-(4-hydroxyphenyl)prop-2-en-1-one (2.58 g, 10 mmol), and K_2CO_3 (1.38, 10 mmol) in anhydrous DMF (20 mL) after 14 h as pale brown solid (3.74 g, 83%); m.p.: 182–184 °C,

^{1}H NMR ($CDCl_3$, 400 MHz): $\delta_{ppm} = 7.98$ (d, $J = 8.4$ Hz, 2H, aryl), 7.84 (d, $J = 15.6$ Hz, 1H, C(O)–CH=CH), 7.73 (d, $J = 8.4$ Hz, 2H, aryl), 7.50–7.485(complex, 3H, C(O)–CH=CH, aryl), 7.42 (d, $J = 8.4$ Hz, 2H, aryl), 3.90 (s, 3H, N(7)-CH_3), 3.47 (s, 3H, N(3)-CH_3), 3.41 (s, 3H, N(1)-CH_3). ^{13}C NMR ($CDCl_3$, 100 MHz): δ_{ppm} = 188.89, 154.87, 152.73, 151.59, 145.71, 143.83, 139.39, 136.32, 132.20, 130.03, 129.90, 129.00, 121.63, 119.88, 116.10, 103.92, 30.53, 29.91, 27.89. IR (KBr): 3070, 2974, 1703, 1694, 1656, 1563, 1471, 1269, 1065, 850 cm^{-1}. MS (EI): m/z (%) = 450 (28.7) [M^+]. Anal. calc. for $C_{23}H_{19}ClN_4O_4$: C, 61.27; H, 4.25; N, 12.43; found: C, 61.02; H, 4.38; N, 12.27.

Data availability

The data pertaining to this manuscript are available upon request.

Conflicts of interest

The authors have declared no conflict of interest.

Acknowledgements

The authors wish to thank the Shiraz University of Technology research council for partial support of this work.

References

1 C. de Martel, D. Georges, F. Bray, J. Ferlay and G. M. Clifford, Global burden of cancer attributable to infections in 2018: a worldwide incidence analysis, *Lancet Glob. Health*, 2020, **8**, e180–e190.
2 E. Bidram, Y. Esmaeili, H. Ranji-Burachaloo, N. Al-Zaubai, A. Zarrabi, A. Stewart and D. E. Dunstan, A concise review on cancer treatment methods and delivery systems, *J. Drug Deliv. Technol.*, 2019, **54**, 101350.
3 S. Akkın, G. Varan and E. Bilensoy, A review on cancer immunotherapy and applications of nanotechnology to chemoimmunotherapy of different cancers, *Molecules*, 2021, **26**, 3382.
4 J. Zugazagoitia, C. Guedes, S. Ponce, I. Ferrer, S. Molina-Pinelo and L. Paz-Ares, Current challenges in cancer treatment, *Clin. Ther.*, 2016, **38**, 1551–1566.
5 S. h. Wang, Y. Liu, Y. Feng, J. Zhang, J. Swinnen, Y. Li and Y. Ni, A review on curability of cancers: more efforts for novel therapeutic options are needed, *Cancers*, 2019, **11**, 1782.
6 M. A. Shalaby, S. A. Rizk and A. M. Fahim, Synthesis, reactions and application of chalcones: a systematic review, *Org. Biomol. Chem.*, 2023, **21**, 5317–5346.
7 C. Zhuang, W. Zhang, C. Sheng, W. Zhang, C. Xing and Z. Miao, Chalcone: a privileged structure in medicinal chemistry, *Chem. Rev.*, 2017, **117**, 7762–7810.
8 S. Narwal, B. Devi, T. Dhanda, S. Kumar and S. Tahlan, Exploring chalcone derivatives: synthesis and their therapeutic potential, *J. Mol. Struct.*, 2024, **1303**, 137554.
9 M. N. Gomes, E. N. Muratov, M. Pereira and J. C. Peixoto, Chalcone derivatives: promising starting points for drug design, *Molecules*, 2017, **22**, 1210.
10 K. Mezgebe, Y. Melaku and E. Mulugeta, Synthesis and pharmacological activities of chalcone and its derivatives bearing N-heterocyclic scaffolds: a review, *ACS Omega*, 2023, **8**, 19194–19211.
11 K. Dzobo, The role of natural products as sources of therapeutic agents for innovative drug discovery, *Compr. Pharm.*, 2022, **2**, 408–422.
12 B. G. Katzung, *Basic & Clinical Pharmacology*, Lange Medical Publications, McGraw-Hill Companies, 14 edn, 2018.
13 T. M. McLellan, J. A. Caldwell and H. R. Lieberman, A review of caffeine's effects on cognitive, physical and occupational performance, *Neurosci. Biobehav. Rev.*, 2016, **71**, 294–312.
14 N. Singh, A. K. Shreshtha, M. S. Thakur and S. Patra, Xanthine scaffold: scope and potential in drug development, *Heliyon*, 2018, **4**, e00829.
15 M. N. Soltani Rad, S. Behrouz, S. Aghajani, M. Behrouz, E. Zarenezhad and A. Ghanbariasad, Design, synthesis, anticancer and *in silico* assessment of 8-caffeinyl-triazolylmethoxy hybrid conjugate, *RSC Adv.*, 2023, **13**, 3056–3070.
16 B. Strydom, J. J. Bergh and J. P. Petzer, 8-Aryl- and alkyloxycaffeine analogues as inhibitors of monoamine oxidase, *Eur. J. Med. Chem.*, 2011, **46**, 3474–3485.
17 M. M. van der Walt and G. Terre'Blanche, Selected C8 two-chain linkers enhance the adenosine A_1/A_{2A} receptor affinity and selectivity of caffeine, *Eur. J. Med. Chem.*, 2017, **125**, 652–656.
18 A. A. Kadi, K. E. H. El-Tahir, Y. Jahng and A. F. M. Motiur Rahman, Synthesis, biological evaluation and structure activity relationships (SARs) study of 8-(substituted) aryloxycaffeine, *Arab. J. Chem.*, 2019, **12**, 2356–2364.
19 A. H. Alkhzem, T. J. Woodman and I. S. Blagbrough, Design and synthesis of hybrid compounds as novel drugs and medicines, *RSC Adv.*, 2022, **12**, 19470–19484.
20 B. Meunier, Hybrid molecules with a dual mode of action: dream or reality?, *Acc. Chem. Res.*, 2008, **41**, 69–77.
21 M. d. O. Pedrosa, R. M. D. d. Cruz, J. d. O. Viana, R. O. d. Moura, H. M. Ishiki, J. M. B. Filho, M. F. F. M. Diniz, M. T. Scotti, L. Scotti and F. J. B. Mendonca, Hybrid compounds as direct multitarget ligands: a review, *Curr. Top. Med. Chem.*, 2017, **17**, 1044–1079.
22 M. N. Soltani Rad and S. Maghsoudi, Two-step three-component process for one-pot synthesis of 8-alkylmercaptocaffeine derivatives, *RSC Adv.*, 2016, **6**, 70335–70342.
23 M. N. Soltani Rad, S. Behrouz, K. Zokaei, M. Behrouz, A. Ghanbariasad and E. Zarenezhad, Synthesis of some novel 8-(4-alkylpiperazinyl) caffeine derivatives as potent anti-leishmania agents, *Bioorg. Chem.*, 2022, **128**, 106062.
24 M. N. Soltani Rad, S. Behrouz, K. Shahbazkhani, M. Behrouz, E. Zarenezhad and A. Ghanbariasad, Design, synthesis, anticancer and *in silico* assessment of 8-piperazinyl

caffeinyl-triazolylmethyl hybrid conjugates, *RSC Adv.*, 2023, **13**, 24656–24673.
25 L. Claisen and A. Claparède, Condensationen von ketonen mit aldehyden, *Ber. Dtsch. Chem. Ges.*, 1881, **14**, 2460–2468.
26 X. Zhang, Y. Q. Li, C. Qian, L. An, W. Wang, X. F. Li, X. Z. Shao and Z. Lia, Research progress of catalysts for aldol condensation of biomass based compounds, *RSC Adv.*, 2023, **13**, 9466–9478.
27 E. Caputo, L. Maiorana, V. Vasta, F. M. Pezzino, S. Sunkara, K. Wynne, G. Elia, F. M. Marincola, J. A. McCubrey, M. Libra, S. Travali and M. Kane, Characterization of human melanoma cell lines and melanocytes by proteome analysis, *Cell Cycle*, 2011, **10**, 2924–2936.
28 Ș. Comșa, A. M. Cimpean and M. Raica, The story of MCF-7 breast cancer cell line: 40 years of experience in research, *Anticancer Res.*, 2015, **35**, 3147–3154.
29 Y.-C. Lin, M. Boone, L. Meuris, I. Lemmens, N. Van Roy, A. Soete, J. Reumers, M. Moisse, S. Plaisance, R. Drmanac, J. Chen, F. Speleman, D. Lambrechts, Y. Van de Peer, J. Tavernier and N. Callewaert, Genome dynamics of the human embryonic kidney 293 lineage in response to cell biology manipulations, *Nat. Commun.*, 2014, **5**, 4767.
30 **https://en.wikipedia.org/wiki/Folate**, accessed 11 June 2024.
31 B. Chabner, and D. L. Longo, *Cancer Chemotherapy and Biotherapy Principles and Practice*, Oxford University press, Wolters Kluwer Health/Lippincott Williams & Wilkins, 5th edn, 2011.
32 L. Genestier, R. Paillot, L. Quemeneur, K. Izeradjene and J. P. Revillard, Mechanisms of action of methotrexate, *Immunopharmacology*, 2000, **47**, 247–257.
33 I. Puzanov, R. K. Amaravadi, G. A. McArthur, K. T. Flaherty, P. B. Chapman, J. A. Sosman, A. Ribas, M. Shackleton, P. Hwu, B. Chmielowski, K. B. Nolop, P. S. Lin and K. B. Kim, Long-term outcome in BRAF (V600E) melanoma patients treated with vemurafenib: patterns of disease progression and clinical management of limited progression, *Eur. J. Cancer*, 2015, **51**, 1435–1443.
34 *Molegro Virtual Docker, Version 6.0.0*, CLC Bio, 8200, Aarhus N, Denmark, 2012.
35 G. Marcou and D. Rognan, Optimizing fragment and scaffold docking by use of molecular interaction fingerprints, *J. Chem. Inform. Model*, 2007, **47**, 195–207.
36 V. Cody, J. R. Luft and W. Pangborn, Understanding the role of Leu22 variants in methotrexate resistance: comparison of wild-type and Leu22Arg variant mouse and human dihydrofolate reductase ternary crystal complexes with methotrexate and NADPH, *Acta Cryst.*, 2005, **D61**, 147–155.
37 R. J. Bienstock, *Library Design, Search Methods, and Applications of Fragment-Based Drug Design*, A.C.S., Washington, 2011.
38 C. A. Lipinski, F. Lombardo, B. W. Dominy and P. J. Feeney, Experimental and computational approaches to estimate solubility and permeability in drug discovery and development settings, *Adv. Drug Deliv. Rev.*, 2001, **46**, 3–25.
39 *PreADMET online server*, **https://preadmet.webservice.bmdrc.org/adme**, accessed 2 June 2024.
40 *OSIRIS Property Explorer*, **https://www.organic-chemistry.org/prog/peo**, accessed 2 June 2024.
41 *SwissADME online software*, **https://www.swissadme.ch/index.php**, accessed 2 June 2024.
42 S. Grimme, J. Antony, S. Ehrlich and H. Krieg, A consistent and accurate *ab initio* parametrization of density functional dispersion correction (DFT-D) for the 94 elements H-Pu, *J. Chem. Phys.*, 2010, **132**, 154104.
43 T. Mosmann, Rapid colorimetric assay for cellular growth and survival: application to proliferation and cytotoxicity assays, *J. Immunol. Methods*, 1983, **65**, 55–63.
44 M. J. Frisch, G. W. Trucks, H. B. Schlegel, G. E. Scuseria, M. A. Robb, J. R. Cheeseman, *et al.*, *Gaussian 09, Revision D.01*, Gaussian, Inc., Wallingford CT, 2013.
45 J. J. P. Stewart, Application of the PM6 method to modeling the solid state, *J. Mol. Model.*, 2008, **14**, 499–535.